NASA CONTRACTOR REPORT

NASA CR-2573

ANALYSIS OF HELICOPTER ROTOR BLADE TORSIONAL OSCILLATIONS DUE TO STALL

Peter Crimi

Prepared by
AVCO SYSTEMS DIVISION
Wilmington, Mass. 01887
for Langley Research Center
and U.S. Army Air Mobility R&D Laboratory

NATIONAL AERONAUTICS AND SPACE ADMINISTRATION • WASHINGTON, D. C. • SEPTEMBER 1975

1. Report No.	2. Government Accession No.	3. Recipient's Catalog No.
NASA CR-2573		

4. Title and Subtitle	5. Report Date
ANALYSIS OF HELICOPTER ROTOR BLADE TORSIONAL OSCILLATIONS DUE TO STALL	September 1975
	6. Performing Organization Code

7. Author(s)	8. Performing Organization Report No.
Peter Crimi	
	10. Work Unit No.

9. Performing Organization Name and Address	11. Contract or Grant No.
AVCO Systems Division Wilmington, Massachusetts 01887	NAS1-12853
	13. Type of Report and Period Covered
12. Sponsoring Agency Name and Address	Contractor Report
National Aeronautics and Space Administration Washington, D.C. 20546	14. Sponsoring Agency Code

15. Supplementary Notes

The contract research which has led to the results in this report was financially supported by USAAMRDL (Langley Directorate). This is a final report.

16. Abstract

An analysis of stall-induced helicopter rotor blade torsional oscillations was carried out, the primary objectives being to predict the onset and severity of the oscillations and their relationship to aircraft and blade parameters. Blade flapping, flapwise bending and torsional degrees of freedom were taken into account, with radial variation in aerodynamic loading determined from a previously developed dynamic stall model, using a strip approximation.

Results of analyses were compared with data from flight tests of two different helicopters. The severity of torsional oscillations and their relation to aircraft forward speed agreed fairly well, while the radial and azimuthal extent of stall and the azimuthal variation of section loading were in good agreement.

Analyses were carried out while parametrically varying blade vibrational characteristics. It was found that the amplitudes of the higher harmonics of torsional oscillations can be significantly reduced by either reducing the torsional natural frequency or introducing viscous damping in the torsional degree of freedom.

A preliminary investigation was also carried out to determine the feasibility and practicality of alleviating the stall problem by means of boundary layer control. The results indicate that boundary layer control would be effective in reducing the higher harmonics of torsional oscillations due to stall and that its implementation would not require excessive power or suction rates.

17. Key Words (Suggested by Author(s))	18. Distribution Statement
Helicopter rotor, Aeroelasticity, Dynamic stall, Torsional stability	Unclassified - Unlimited Subject category 02

19. Security Classif. (of this report)	20. Security Classif. (of this page)	21. No. of Pages	22. Price*
Unclassified	Unclassified	56	$4.25

*For sale by the National Technical Information Service, Springfield, Virginia 22161

ANALYSIS OF HELICOPTER ROTOR BLADE TORSIONAL OSCILLATIONS DUE TO STALL

By Peter Crimi
Avco Systems Division

SUMMARY

An analysis of stall-induced helicopter rotor blade torsional oscillations was carried out, the primary objectives being to predict the onset and severity of the oscillations and their relationship to aircraft and blade parameters. Blade flapping, flapwise bending and torsional degrees of freedom were taken into account, with radial variation in aerodynamic loading determined from a previously developed dynamic stall model, using a strip approximation.

Results of analyses were compared with data from flight tests of two different helicopters. The severity of torsional oscillations and their relation to aircraft forward speed agreed fairly well, while the radial and azimuthal extent of stall and the azimuthal variation of section loading were in good agreement.

Analyses were carried out while parametrically varying blade vibrational characteristics. It was found that the amplitudes of the higher harmonics of torsional oscillations can be significantly reduced by either reducing the torsional natural frequency or introducing viscous damping in the torsional degree of freedom.

A preliminary investigation was also carried out to determine the feasibility and practicality of alleviating the stall problem by means of boundary layer control. The results indicate that boundary layer control would be effective in reducing the higher harmonics of torsional oscillations due to stall and that its implementation would not require excessive power or suction rates.

INTRODUCTION

A problem currently of particular concern in helicopter design and operation is the occurrence of large-amplitude oscillatory blade torsional deflections and control-linkage loads caused by stall at high forward speed. The oscillations effectively limit the speed of the aircraft because the control linkages are not able to withstand sustained oscillatory loading of that severity (Ref. 1).

Numerous studies of various aspects of the problem have been conducted in the past several years. Many of these have been concerned with the process of unsteady airfoil stall and its relationship to excitation of the torsional oscillations. Experimental studies (Refs. 2-5, for example) have shown that the dominant feature of dynamic stall is the development and growth of a region of vortical flow, starting from the leading edge, which induces lift considerably in excess of what is achieved statically and, of particular importance to the rotor problem, causes a rapid rearward shift in the center of pressure, resulting in severe transient nose-down moments. Analyses of unsteady stall of two-dimensional airfoils with viscous effects taken into account empirically have been performed (Refs. 6 and 7). More recently, an analytical model of unsteady stall was developed which accounts for interaction of the viscous and inviscid flows (Refs. 8 and 9). This theory, which shows quite good qualitative and fair quantitative agreement with measurements of airfoil loading, was employed in the study reported here, and is described briefly in the next section.

Considerable research has also been directed specifically to the rotor problem. Results of wind tunnel and flight tests of rotors undergoing stall-induced torsional oscillations are reported in Refs. 10 through 13. Analytical studies utilizing empirical aerodynamic representations are presented in Refs. 14 and 15. The analyses are for the most part in reasonably good agreement with the tests, but the use of empirical methods restricts their applicability. The study reported in Ref. 16 employed the analytic dynamic stall model of Ref. 8, but a two-dimensional elastomechanical system was used to approximate that of a rotor blade, the objectives being primarily to qualitatively evaluate and determine the interrelationships of different rotor aeroelastic instabilities.

This study was specifically directed to predicting rotor blade torsional oscillations due to stall and their relationship to flight conditions and rotor parameters, using a more realistic aeroelastic model which includes an analytic representation of unsteady stall and accounts for radial variations in aerodynamic loading. Responses of the blade in flapping, flapwise bending and torsion have been analyzed by forward integration in time with the

aerodynamic loading evaluated at either five or six radial stations, using the strip approximation and assuming uniform inflow. Results of analyses of specific rotor configurations have been compared with flight test data, and the effect of parametric variations in blade vibrational characteristics examined. In addition, a preliminary assessment has been made of the possible use of boundary layer control in the suppression of torsional oscillations.

SYMBOLS

b	blade semichord, m
C_l	blade section lift coefficient, ratio of lift per unit span to $\rho U^2 b$
C_m	blade section moment coefficient, ratio of moment per unit span about quarter-chord, positive nose up, to $2 \rho U^2 b^2$
C_p	pressure coefficient, ratio of pressure, less free-stream pressure, to $\rho U^2/2$
C_Q	suction coefficient, $C_Q = Q/(Uc)$
C_T	rotor thrust coefficient, ratio of thrust to $\pi \rho \Omega^2 R^4$
c	blade chord, m
f_Θ	first coupled torsion-control deflection mode shape
f_ϕ	first flapwise bending mode shape
$\overline{GJ}$	average blade torsional stiffness, $N\text{-}m^2$
$\dot{h}$	section plunging rate, m/s
I	ratio of section moment of inertia to $M_B R$
k_c	control stiffness, N-m/rad
k_m	mass ratio, $k_m = \rho R^3/M_B$
L_c	pushrod moment arm with respect to pitch axis, m
l_c	length of controlled blade segment, m
M_B	blade mass, kg
M_B'	blade mass per unit span, kg/m
m	dimensionless mass per unit span, $m = R M_B'/M_B$
N_B	number of blades
P_s	total power required by boundary layer control system, hp

Q	suction rate per unit span, m^2/s
Q_{TOT}	total suction rate per blade, m^3/s
q_s	magnitude of fluid velocity at the edge of the boundary layer at the separation point, m/s
R	rotor radius, m
Re	Reynolds number, $Re = Uc/\nu$.
r	blade-fixed radial coordinate, m
r_A	inner radius of controlled segment, m
r_B	outer radius of controlled segment, m
r_c	radius at center of controlled segment, m
r_o	ratio of blade root cut-out radius to R
s	dimensionless radial coordinate, $s = r/R$
U	magnitude of free-stream velocity relative to blade section, m/s
V_f	helicopter forward speed, m/s
W	helicopter gross weight, N
w_i	wake-induced inflow, m/s
(x, y, z)	shaft-fixed rotor coordinates, m
x_l	chordal coordinate with origin at the leading edge, positive aft, m
x_m	ratio of blade section mass center offset, positive aft, to R
x_R	location of downstream end of trapped-air region
x_s	location of separation point
α	angle of attack, deg
α_s	shaft angle with respect to vertical, positive aft, rad

β	flapping angle, rad
Δ_p	possible increase in C_p across leading-edge bubble
Δ_r	required increase in C_p across leading-edge bubble
δ	ratio of flapping hinge offset to R
ζ	viscous damping coefficient in torsion, fraction of critical
Θ	angle between blade section chord line and rotor plane, rad
Θ_o	blade root pitch angle, rad
Θ_1	blade tip angular deflection due to first coupled torsion-control deflection mode, rad
μ	advance ratio, $\mu = V_f/(\Omega R)$
ν	kinematic viscosity of air, m^2/s
ξ_c	stall parameter, $\xi_c = (1 - \Delta_p/\Delta_r)^{1/2}$
ρ	air density, kg/m^3
Φ	blade tip deflection due to first flapwise bending mode, m
ψ	blade azimuth angle, deg or rad
Ω	rotor angular speed, rad/sec
ω_{2_o}	ratio of nonrotating bending vibration frequency to Ω
ω_2	ratio of rotating bending vibration frequency to Ω
ω_{3_o}	ratio of nonrotating torsion-control deflection vibration frequency to Ω
ω_3	ratio of rotating torsion-control deflection vibration frequency to Ω

FORMULATIONS

System Analyzed

The motions of the rotor blade are referred to shaft-fixed coordinates (x, y, z), with the x-axis directed downwind, as indicated in Fig. 1. Blade deflection due to flapping and flapwise bending at radial position r is $\beta r + f_\phi(r)\,\phi$, where β is flapping angle, ϕ is bending deflection at the tip (r = R) and f_ϕ is the mode shape of the first flapwise bending mode (see Fig. 1).

The flow relative to a blade section at radial station r, with the blade at azimuth angle ψ, is as shown in Fig. 2. The plunging rate $\dot{h}$ indicated in the figure results from blade flapping and flapwise bending, and is given by

$$\frac{\dot{h}}{\Omega R} = -\left[\left(\frac{r}{R} - \delta\right)\frac{d\beta}{d\psi} + f_\phi\,\frac{d\phi}{d\psi} + \mu\,(\beta + f'_\phi\,\phi)\cos\psi\right]$$

The blade section angle Θ, measured with respect to the x-y plane, is the sum of the built-in twist $f_o(r)$, blade root pitch setting $\Theta_o(\psi)$ and torsional deflection $f_\Theta\,\Theta_1$, Θ_1 being the torsional deflection at the tip and f_Θ the mode shape of the first coupled torsion-control deflection mode. The section pitch rate is given by

$$\frac{\dot{\theta}}{\Omega} = \frac{d\theta_o}{d\psi} + f_\theta(r)\,\frac{d\theta_1}{d\psi} + \beta + f'_\phi\,\phi$$

The last two terms in the above expression derive from the component of rotor angular velocity parallel to the blade elastic axis.

Aerodynamic Loading

The radial distribution of blade section lift and moment were obtained by applying the theory of Refs. 8 and 9 stripwise at up to six radial locations. It was necessary to restrict the analysis by only allowing for the occurrence of leading-edge stall, even though the theory can take account of trailing-edge stall as well, in order to keep computer storage and time requirements within practical bounds. Since, as discussed further in the next section, the

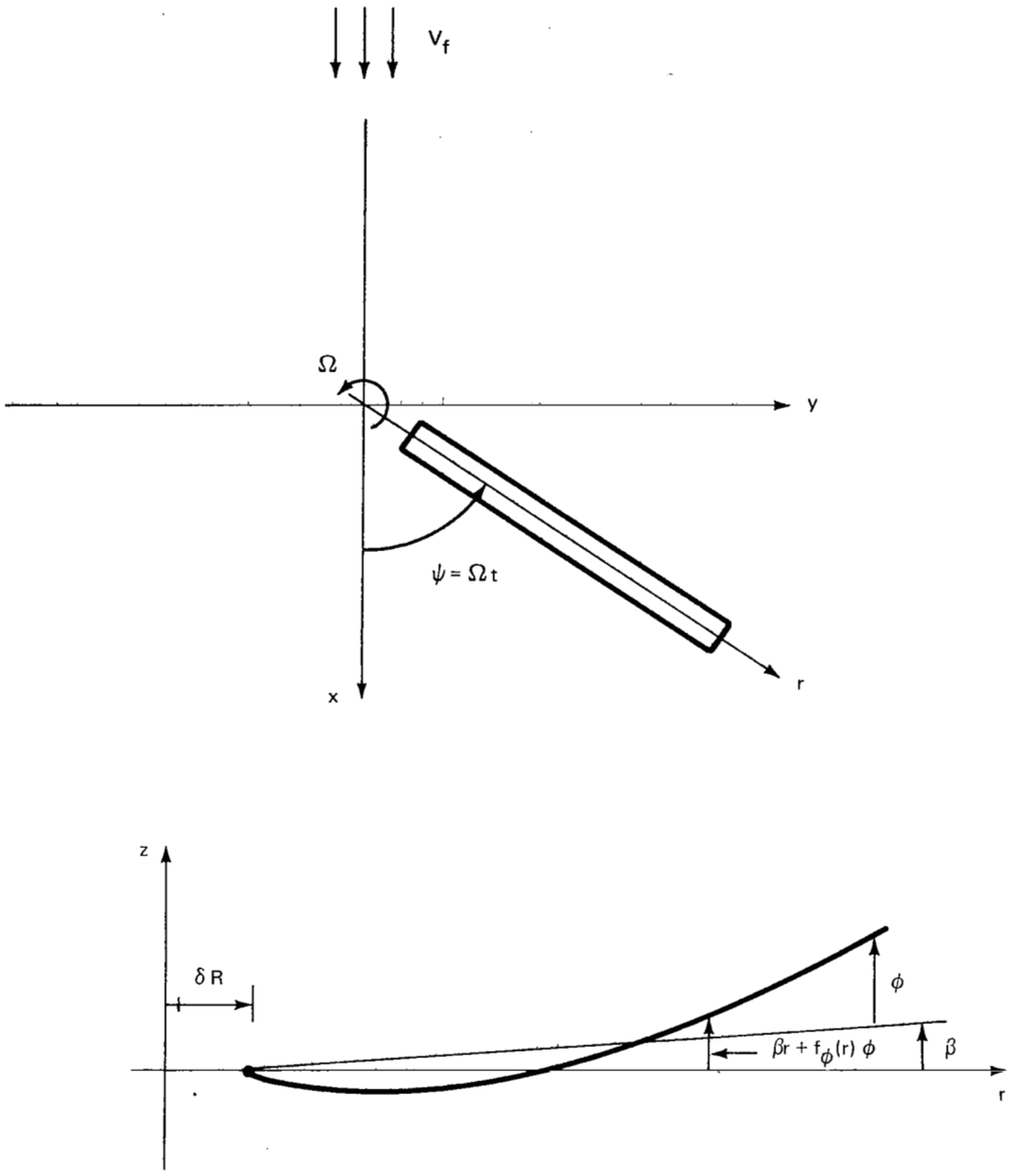

Figure 1 ROTOR COORDINATE SYSTEM

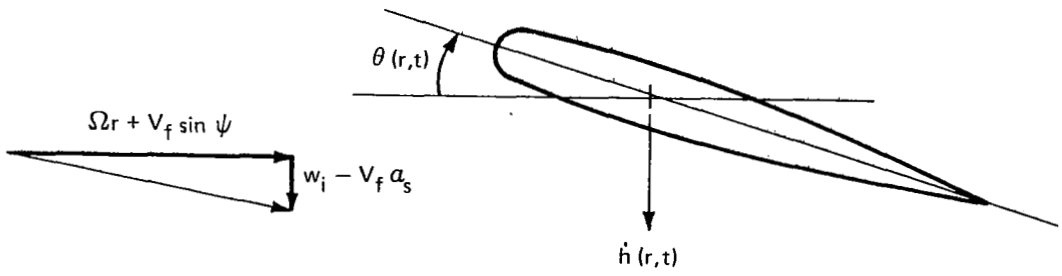

Figure 2 FLOW RELATIVE TO A BLADE SECTION

computed loading does agree quite well with flight test data, this simplification apparently was a reasonable one.

The flow elements represented in the analysis are sketched in Fig. 3. When the airfoil is not stalled (Fig. 3a) these are: (1) the laminar boundary layer from the stagnation point to separation near the leading-edge, (2) the small leading-edge separation bubble, and (3) a potential flow, including a vortex wake generated by the variation with time of the circulation about the airfoil. When the airfoil is stalled, as indicated in Fig. 3b, the flow elements are: (1) the laminar boundary layer, (2) a trapped-air region extending from the separation point to the pressure recovery point, and (3) a potential flow external to the airfoil and trapped-air region, again including a vortex wake. The analytic representations of these elements are described briefly below. Details are given in Refs. 8 and 9.

Potential Flow. — Given the airfoil section characteristics and motions, together with the distribution of pressure in the trapped-air region if the airfoil is stalled, the flow and pressure over the airfoil must be determined to compute the integrated load and analyze the boundary layer. The problem was formulated by imposing linearized boundary conditions of flow tangency and pressure, using a perturbation velocity potential derived from source and vortex distributions. The resulting coupled set of singular integral equations is solved by casting the singularity distributions in series form and solving for the unknown coefficients by imposing boundary conditions at prescribed points. A consistent second-order correction to the linearized solution is then calculated and added to the latter solution.

Boundary Layer. — The boundary layer representation of Ref. 8 employs the method of finite differences for unsteady flows with variable step size in both streamwise and normal directions, with the error in each finite-difference approximation the order of the square of the step size. It was determined from preliminary calculations performed for the study reported in Ref. 16 that, at least for leading-edge stall, results are virtually unaffected by assuming quasi-steady flow in the boundary layer. That assumption was therefore employed for all computations, to take advantage of the resulting substantial savings in computer storage requirements and computing time.

Trapped-Air Region. — The function of the model of the trapped-air region is to define the streamwise distribution of pressure in that region, given the locations of the separation and recovery points and the pressure at the recovery point. The region is assumed to consist of a laminar constant-pressure free shear layer from separation to transition, a turbulent constant-pressure mixing region, and a turbulent pressure-recovery region. The laminar shear layer is analyzed by the method of Ref. 17, assuming quasi-steady flow. The turbulent mixing and pressure-recovery regions are

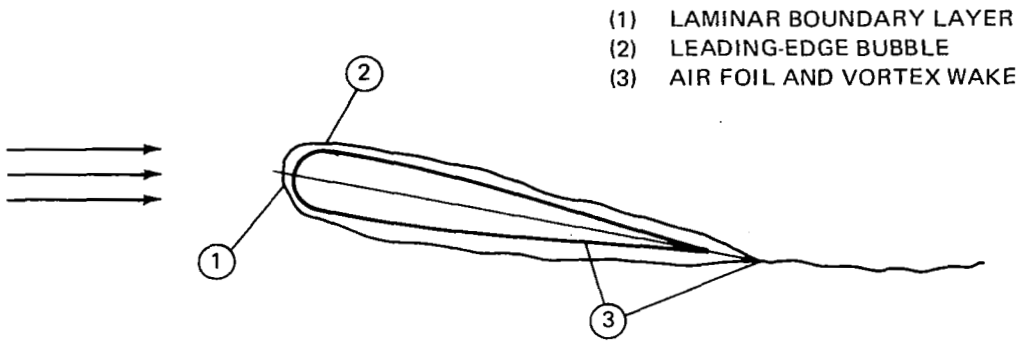

(a) ATTACHED FLOW

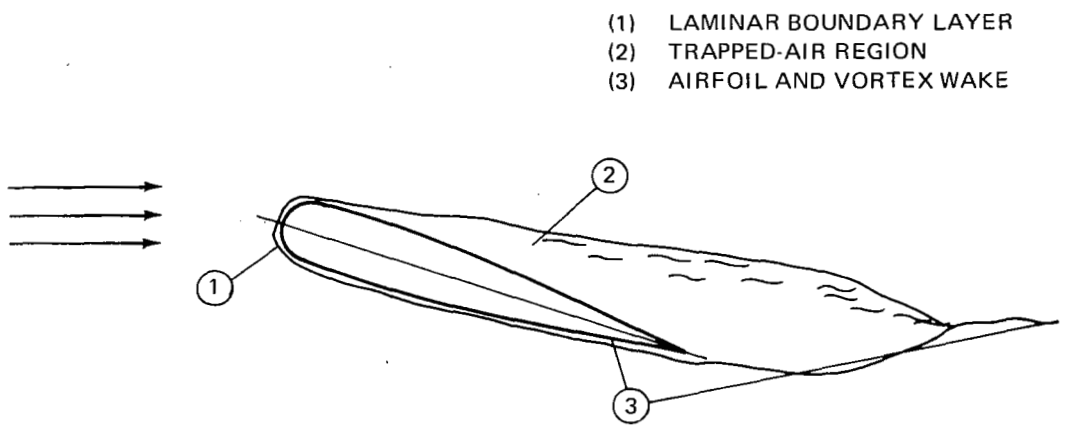

(b) LEADING-EDGE STALL

Figure 3 FLOW ELEMENTS

analyzed using the steady-flow momentum integral and first moment equations. Profile parameters in these regions are assumed to be universal functions of a dimensionless streamwise coordinate, with those functions derived from an exact viscous-inviscid interaction calculation. Matching of approximate solutions for the mixing and pressure-recovery regions at their interface completes the analysis.

Leading-Edge Bubble. — The leading-edge bubble on an unstalled airfoil is analyzed using the same basic relations employed for the trapped-air region. Given the boundary-layer parameters at separation, the length of the bubble and the amount of pressure rise possible, for that length, in the pressure recovery region, are computed. That pressure rise is compared with the rise in pressure in the potential flow over the length of the bubble. If the latter is greater than the former, the bubble is assumed to have burst, and the stall process is initiated.

Loading Calculation Procedure. — Calculation of the loading at a given blade section proceeds by forward integration in time, using the blade motions derived by integrating the equations of motion of the elastomechanical system. If, at a given instant, the blade section is not stalled, the potential flow is computed, and the boundary layer and leading-edge bubble are analyzed to check for bubble bursting. If the section is stalled, the pressure distribution in the trapped-air region is computed, the potential flow evaluated, and the boundary layer is analyzed to locate the separation point. The last two steps are repeated iteratively until assumed and computed separation points agree. Rate of growth of the trapped-air region is determined from an estimate of the rate of fluid entrainment derived from the potential-flow solution. Unstall is determined by first postulating its occurrence and analyzing the leading-edge bubble which would then form to ascertain whether that event did in fact occur.

Elastomechanical Representation

As noted previously, a blade with flapping, flapwise bending and torsional degrees of freedom was analyzed. Using blade azimuth angle ψ as independent variable, the equations of motion for the blade can be written in the following dimensionless form (Ref. 16):

$$\sum_{j=1}^{3} \left[\frac{M_{ij}}{M_{ii}} \frac{d^2 Z_j}{d\psi^2} - \frac{T_{ij}}{M_{ii}} Z_j \right] + \omega_{i_o}^2 Z_i = \frac{F_i}{M_{ii}} , \quad i = 1, 2, 3;$$

where $Z_1 = \beta$, $Z_2 = \phi/R$ and $Z_3 = \Theta_1$. The ω_{i_o}'s are nonrotating, uncoupled natural frequencies ($\omega_{1_o} \equiv 0$). The dimensionless mass and centrifugal force coefficients are given by

$$M_{11} = \int_{\delta}^{1} (s-\delta)^2 \, m \, ds \qquad T_{11} = -\int_{\delta}^{1} s(s-\delta) \, m \, ds$$

$$M_{22} = \int_{\delta}^{1} f_{\phi}^{\,2} \, m \, ds \qquad T_{22} = -\int_{\delta}^{1} \left(\frac{df_{\phi}}{ds}\right)^2 \left[\int_{s}^{1} s_1 \, m \, ds_1\right] ds$$

$$M_{33} = \int_{\delta}^{1} f_{\theta}^{\,2} \, I' \, ds \qquad T_{33} = -M_{33}$$

$$M_{12} = 0 \qquad T_{12} = 0$$

$$M_{13} = -\int_{\delta}^{1} (s-\delta) \, x_m \, f_{\phi} \, m \, ds \qquad T_{13} = -M_{13}$$

$$M_{23} = -\int_{\delta}^{1} f_{\phi} \, f_{\theta} \, x_m \, m \, ds \qquad T_{23} = \int_{\delta}^{1} (s-\delta) \left(\frac{df_{\phi}}{ds}\right) f_{\theta} \, x_m \, m \, ds$$

$$M_{ji} = M_{ij} \qquad T_{ji} = T_{ij}$$

The generalized forces are integrals over the blade span involving section lift and moment:

$$F_1 = k_m \int_{r_o}^{1} \overline{l}\,(s - \delta)\, ds$$

$$F_2 = k_m \int_{r_o}^{1} \overline{l}\, f_\phi \, ds$$

$$F_3 = k_m \int_{r_o}^{1} \overline{m}\, f_\theta \, ds$$

where $\overline{l} = u^2 \frac{b}{R} C_l$

$$\overline{m} = 2u^2 \left(\frac{b}{R}\right)^2 C_m$$

$$u = s + \mu \sin \psi$$

while C_l and C_m are section lift and moment coefficient, respectively.

The computer coding used to evaluate the blade elastomechanical parameters was kept separate from the main computer program. The latter program could, therefore, be employed without difficulty to analyze blades with different hub restraints than the ones treated here.

Analysis Procedure

At a given azimuth position ψ, the section lift and moment coefficients are computed at specified radial position, deriving section plunging rate, pitch angle and pitch rate from the blade response at that azimuth position. The integrals defining the generalized forces are then evaluated. The integrands of those integrals are assumed to vary linearly between the sections at which the load is evaluated and to go to zero parabolically at the blade tip and the blade root.

The integration in azimuth angle ψ (i.e., in time) to obtain blade response caused considerable difficulty in the early stages of the study. The complexity of the aerodynamic representation dictates that the azimuthal step size be as large as possible. Further, the logic involved in evaluating the load at stall onset and during unstall would be extremely difficult to adapt to an integration scheme such as the Runge-Kutta method, which requires trial values of the loading to be computed at intermediate azimuth angles. Therefore, a type of predictor-corrector scheme was devised which avoided computing the loading at a given azimuth position more than once. Specifically, a first estimate of the response at azimuth position $\psi + \Delta\psi$ was obtained by linearly extrapolating the generalized forces, using their values at $\psi - \Delta\psi$ and ψ, and integrating the equations of motion analytically for a linear variation of the forcing functions. The resulting response at $\psi + \Delta\psi$ was used to compute the section loading and corrected values for the generalized forces. Then, the blade response at $\psi + \Delta\psi$ was recomputed, using the corrected values for the generalized forces at $\psi + \Delta\psi$, again assuming a linear variation for the forcing functions.

During initial calculations, the torsional degree of freedom exhibited a numerical instability. After trying various remedies, it was finally determined that the last step in the integration scheme was the one causing the problem. When that step was simply omitted, the numerical problem was eliminated and results of acceptable accuracy were obtained, provided the integration step was no larger than about one-sixth of the period of torsional oscillations. This required computer running times which were considerably greater than had originally been anticipated, but which were still within practical bounds.

For all results presented here, the integration step size was six degrees of azimuth, which gives a minimum of eight steps per cycle of torsional oscillation for the blades analyzed. Typically, one revolution of a blade required about 45 minutes of 360/75 computer time.

RESULTS OF COMPUTATIONS

Configurations Analyzed

For comparison with flight test data, analyses were carried out for both an H-34 and a CH-54B rotor blade. The basic H-34 configuration was used in the investigations of the effects of vibratory characteristics and of boundary layer control. Blade and flight parameters of the two aircraft, obtained primarily from Refs. 11 and 12, are listed in Table 1. Bending and torsion mode shapes for the H-34 are plotted in Fig. 4. The bending mode shape for the CH-54B is very nearly the same as that of the H-34, and the torsion mode shape differs only in the deflection at the root, which is .0909, compared with .0969 for the H-34. Blade bending stiffness and mass distributions are shown in Figs. 5 and 6.

The blades of both aircraft have an NACA 0012 section, modified by a small trailing-edge extension. The blade section is shown in Fig. 7, together with a table of offsets. The static lift and moment coefficient variations with angle of attack, obtained from Ref. 18, are plotted in Fig. 8, together with the computed variations, taken from Ref. 9.

In the calculations, for a given advance ratio, collective pitch angle was first varied parametrically until the desired thrust coefficient was obtained. The value of C_T used for the H-34 is .0057 and for the CH-54B, .010.

Effect of Advance Ratio - Comparison with Flight Test

H-34. — The data from Flight 15 of Ref. 11 were selected for detailed comparison with computed blade response and loading. During this flight, the blades were undergoing severe torsional oscillations due to stall. The aircraft was in level flight at a speed of 105 kts and an advance ratio of .29. The variation with ψ of the blade torsional moment at $r/R = .15$, showing large amplitude oscillations at between 6 and 7 cycles per revolution in the third and fourth quadrants, is plotted in Fig. 9. For comparison, the torsional moment for Flight 13 of Ref. 11 (level flight, $V_f = 99$ kts, $\mu = .27$) is also plotted, there being no evidence of stall-induced oscillations during that flight. The variations of section lift and moment coefficients with ψ for these flights, computed from the data of Ref. 11, are shown in Fig. 10 for r/R of .55, .75, .85, and .95. The loading variations for the higher advance ratio are symptomatic of dynamic stall. The lift coefficient rapidly rises to a value considerably in excess of the maximum static value of about 1.2, while at the same time the moment coefficient drops sharply to a large negative value. The lift coefficient then decreases while the moment coefficient

TABLE 1

BLADE AND FLIGHT PARAMETERS

Parameter	H-34	CH-54B
R - m	8.53	10.97
c - m	.417	.660
δ	.0357	.05
r_o	.143	.27
I'	$.6323 \times 10^{-4}$	1.132×10^{-4}
$\overline{GJ}/R$ - N-m/rad	$.5250 \times 10^{4}$	$.17900 \times 10^{5}$
k_c - N-m/rad	$.790 \times 10^{5}$	$.203 \times 10^{6}$
L_c - m	.203	.216
Ω - rad/s	22.2	19.37
ω_{2_o}	.713	.825
ω_2	2.61	2.67
ω_{3_o}	6.56	7.33
ω_3	6.63	7.40
Twist - deg	-8	-14
M_B - kg	119	215
k_m	5.82	7.54
W - N	51,200	214,000
x_m	0.0	0.0

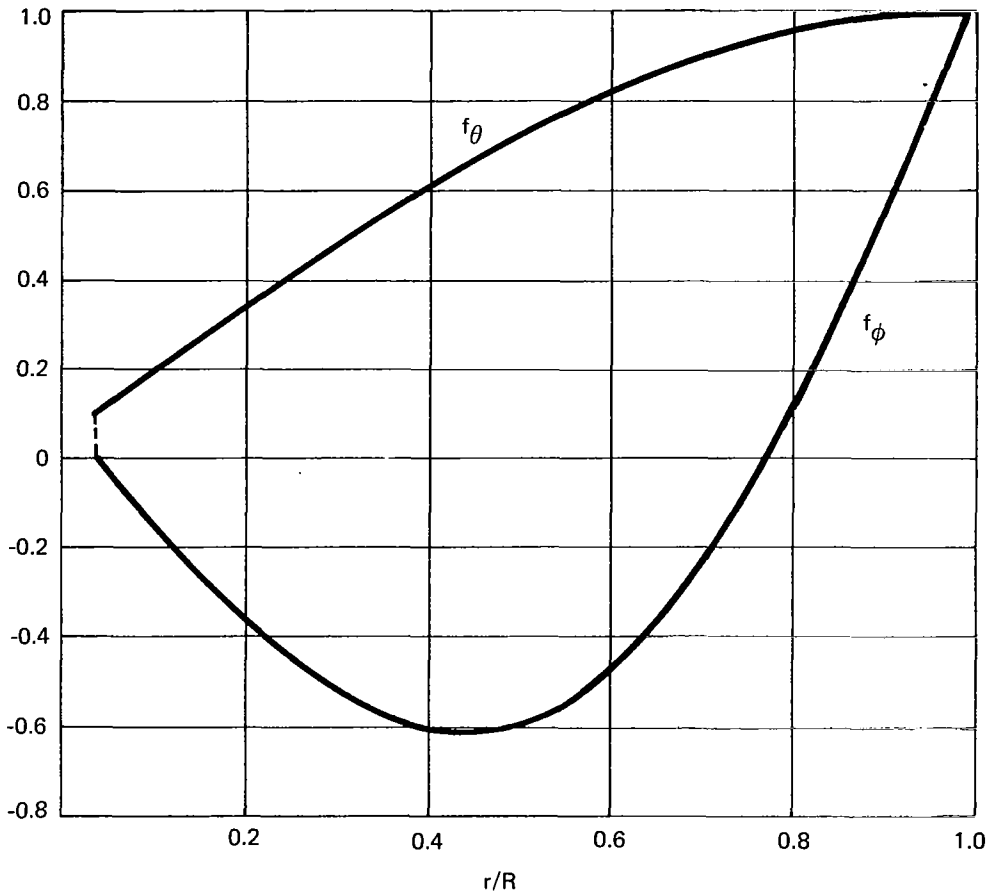

Figure 4 BENDING AND TORSION MODE SHAPES FOR THE H-34 ROTOR BLADE

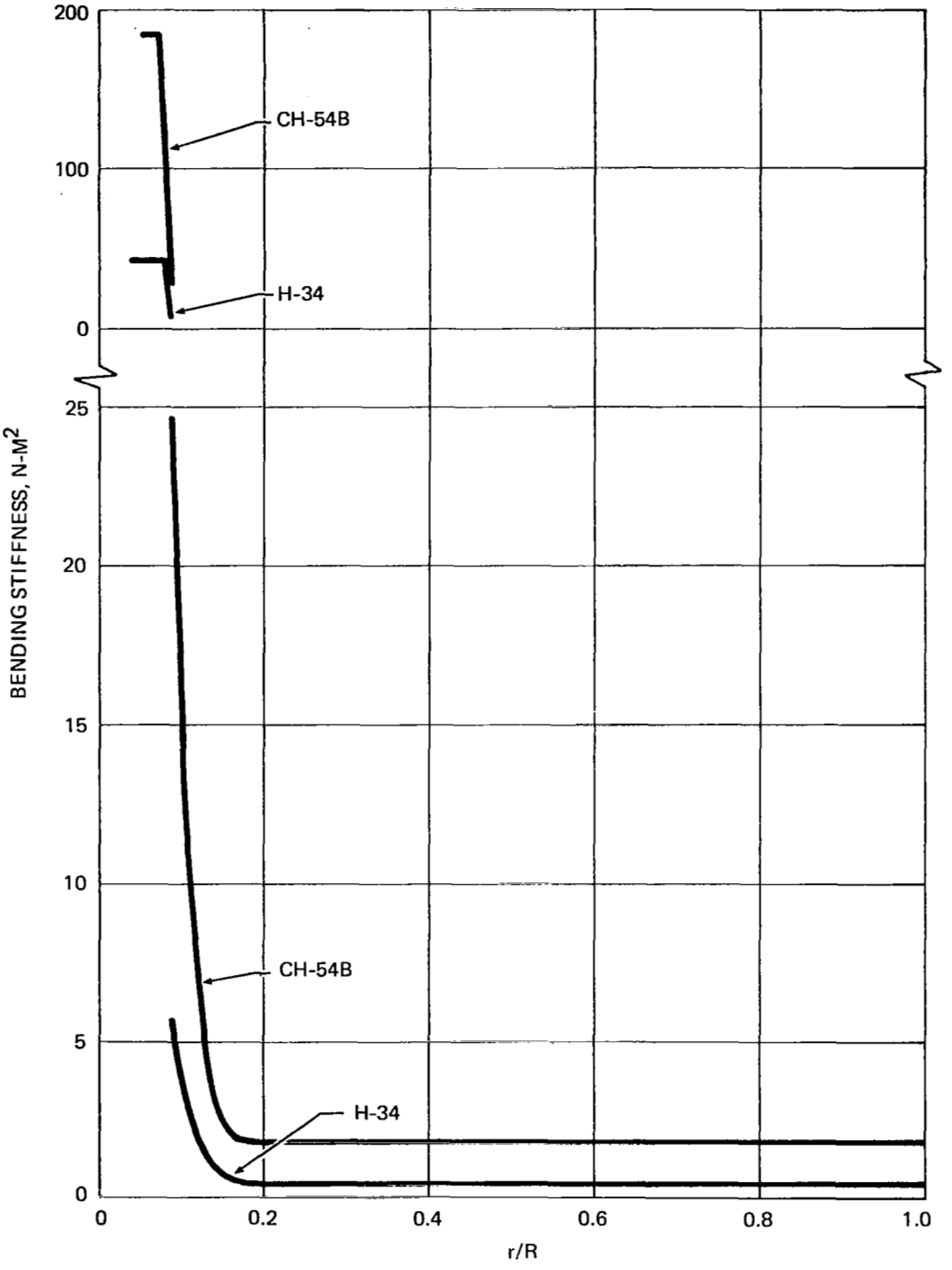

Figure 5 BLADE BENDING STIFFNESS DISTRIBUTIONS

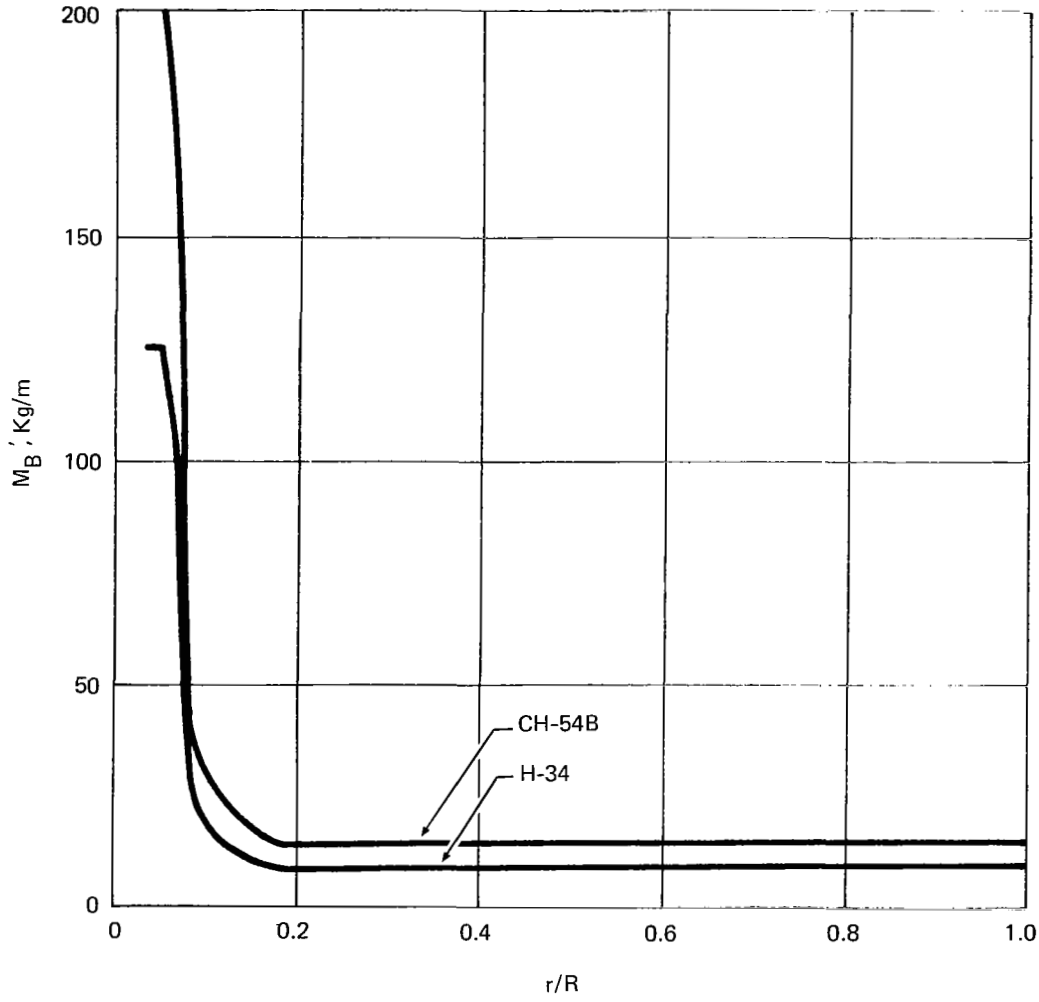

Figure 6 BLADE MASS DISTRIBUTIONS

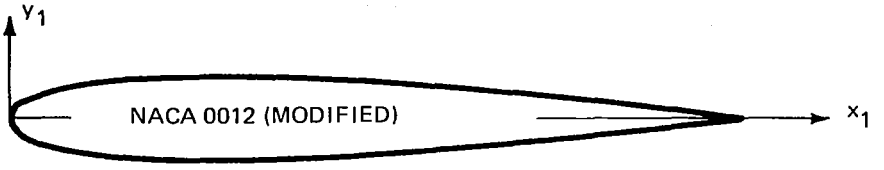

x_1/c	Yu/c
0	0
0.0110	0.0170
0.0220	0.0230
0.0330	0.0270
0.0540	0.0340
0.0760	0.0390
0.1087	0.0445
0.1521	0.0493
0.2065	0.0527
0.2500	0.0542
0.3043	0.0547
0.3478	0.0541
0.4130	0.0520

x_1/c	Yu/c
0.4564	0.0499
0.5000	0.0472
0.5434	0.0439
0.6086	0.0383
0.6521	0.0343
0.6955	0.0300
0.7607	0.0230
0.8042	0.0181
0.8477	0.0127
0.8911	0.0070
0.9346	0.0011
1.000	0.0011

ro/c = 0.0143

Figure 7 AIRFOIL SECTION AND OFFSETS

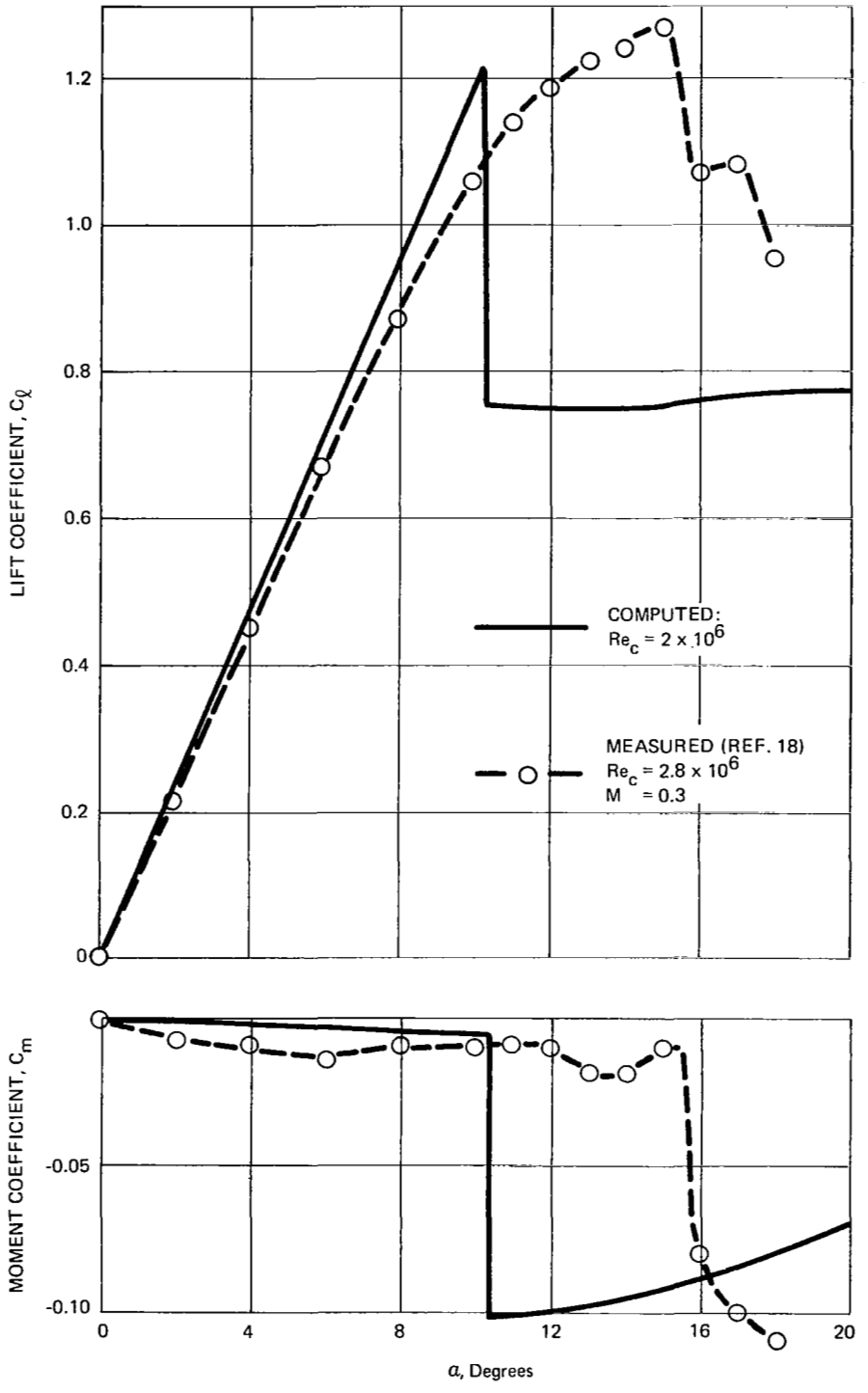

Figure 8 STATIC LIFT AND MOMENT COEFFICIENTS

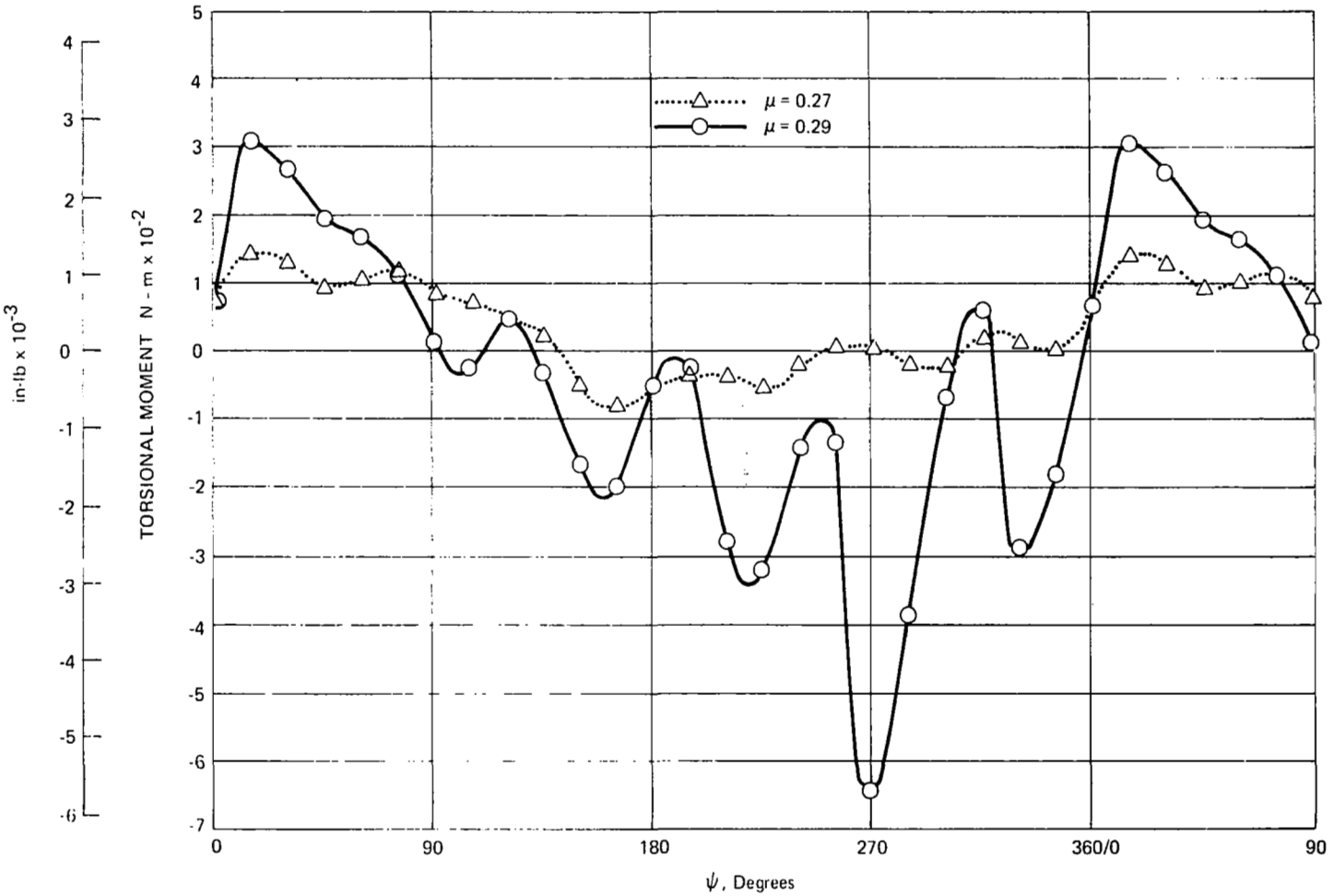

Figure 9 VARIATIONS OF BLADE TORSIONAL MOMENT AT r = 0.15 R DURING H-34 FLIGHT TESTS

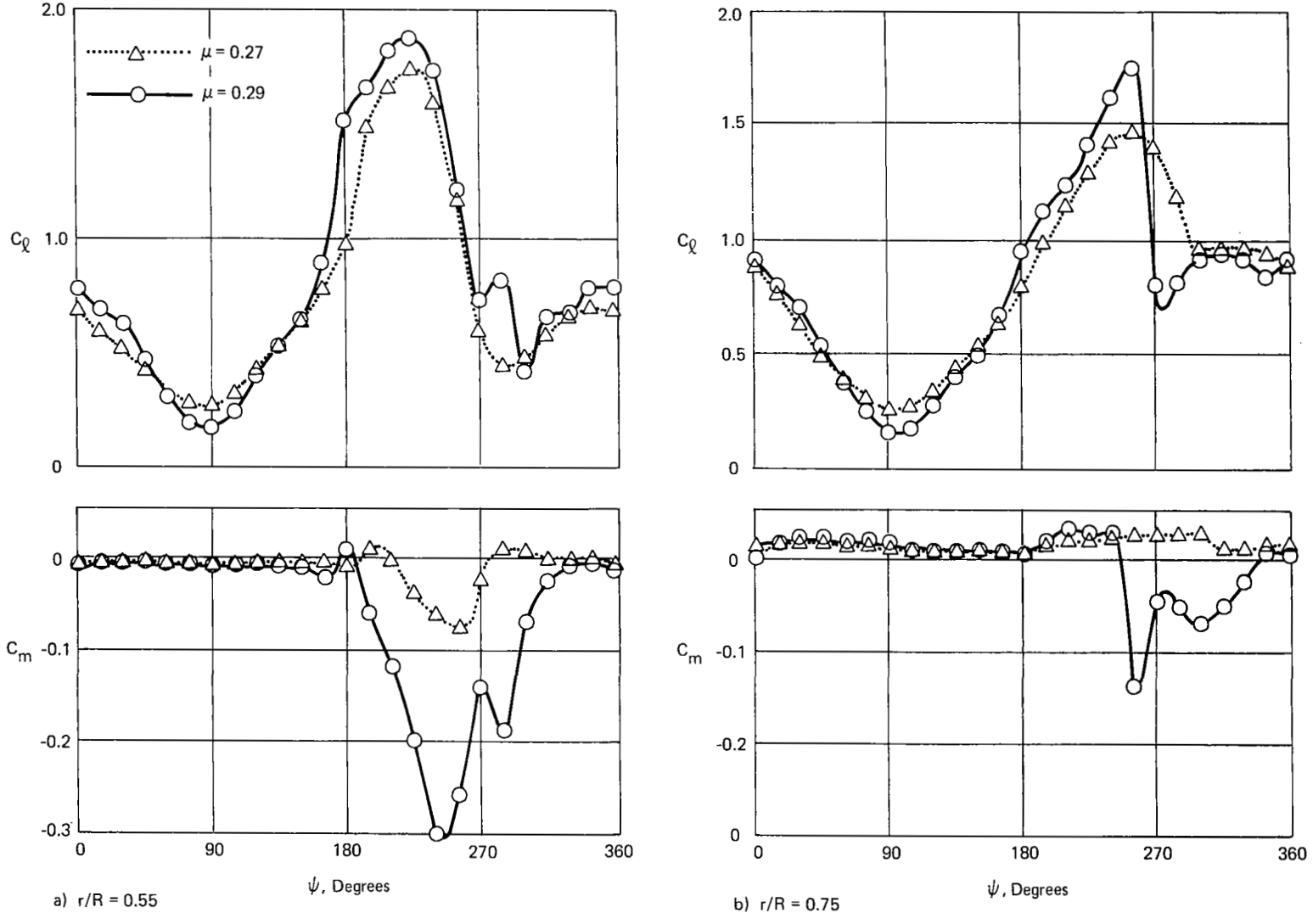

Figure 10 VARIATIONS OF BLADE SECTION LIFT AND MOMENT COEFFICIENTS DURING H-34 FLIGHT TESTS

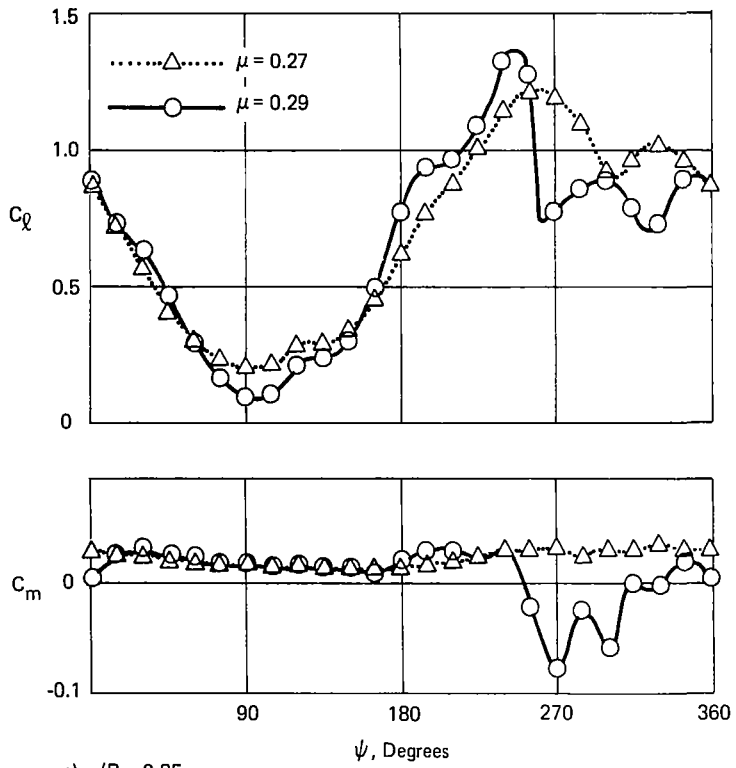

c) r/R = 0.85

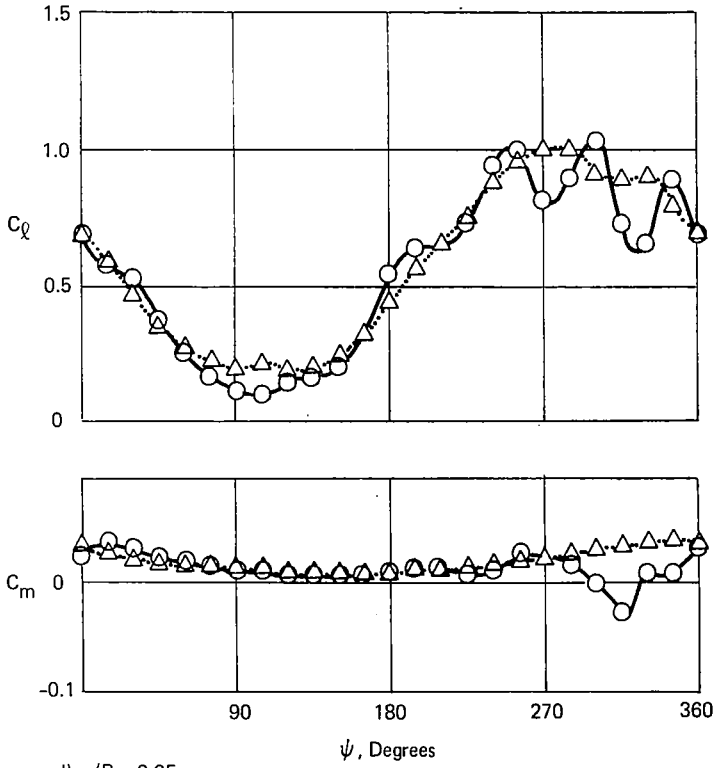

d) r/R = 0.95

Fig. 10 (Concl'd)

rises to a somewhat more moderate value. Unstall is marked by the return of the moment coefficient to near zero.

The results of the analysis of the H-34 blade at $\mu = .27$ are in good agreement, in terms of both the extent of stall and the variation of torsional moment, with the flight test data. Increasing advance ratio brought about the expected increase in blade stall and resulting large-amplitude torsional oscillations, but at a somewhat higher speed than in the flight test, due to a more gradual growth in the stall zone with increasing μ. The computed blade root torsional moments for advance ratios of .31 and .33 as well as .27, are shown in Figs. 11 and 12, together with the flight test results. There is some evidence of torsional oscillations in the fourth quadrant at $\mu = .31$ (Fig. 11) but not as severe as what was measured. At $\mu = .33$ (Fig. 12), oscillations roughly comparable to the measured ones are seen.

To show the relation between the severity of the oscillations and the extent of blade stall, the computed stall zones for advance ratios of .31 and .33 are mapped in Fig. 13, together with the measured stall zone at $\mu = .29$. The computed stall zone for the lower advance ratio is seen to be somewhat smaller than what was measured, with stall reaching to about $r/R = .85$, while the computed extent of stall for $\mu = .33$ is nearly coincident with the flight test results. Thus, a relatively small increase in the radial extent of stall caused a large increase in the amplitude of the torsional oscillations.

The more rapid onset of stall-induced oscillations with increasing seen in the flight test results could be due in part to differences in aircraft gross weight. There is an uncertainty of about 5% in the weight, and hence rotor thrust, reported in Ref. 11, so the data for Flight 15 ($\mu = .29$) could have been taken with the rotor operating at a somewhat higher thrust level than for Flight 13 ($\mu = .27$), thereby causing extensive blade stall at only a slightly higher advance ratio. In any case, because of the good agreement in the extent of stall and severity of the resulting torsional oscillations, in what follows the computed results for $\mu = .33$ will be regarded as comparable to the flight test measurements at $\mu = .29$.

The computed variations of section lift and moment coefficients with ψ for $\mu = .27$ and $\mu = .33$ are shown in Fig. 14. The azimuth positions of stall and unstall have been marked on the abscissa. In comparing these results with the measured loading (Fig. 10), it is seen that the essential features of the unsteady stall process are reproduced. Substantial lift overshoot is accompanied by a rapid drop in moment coefficient, with a partial increase in moment shortly after the drop in lift, followed by a return of the moment to near zero at unstall.

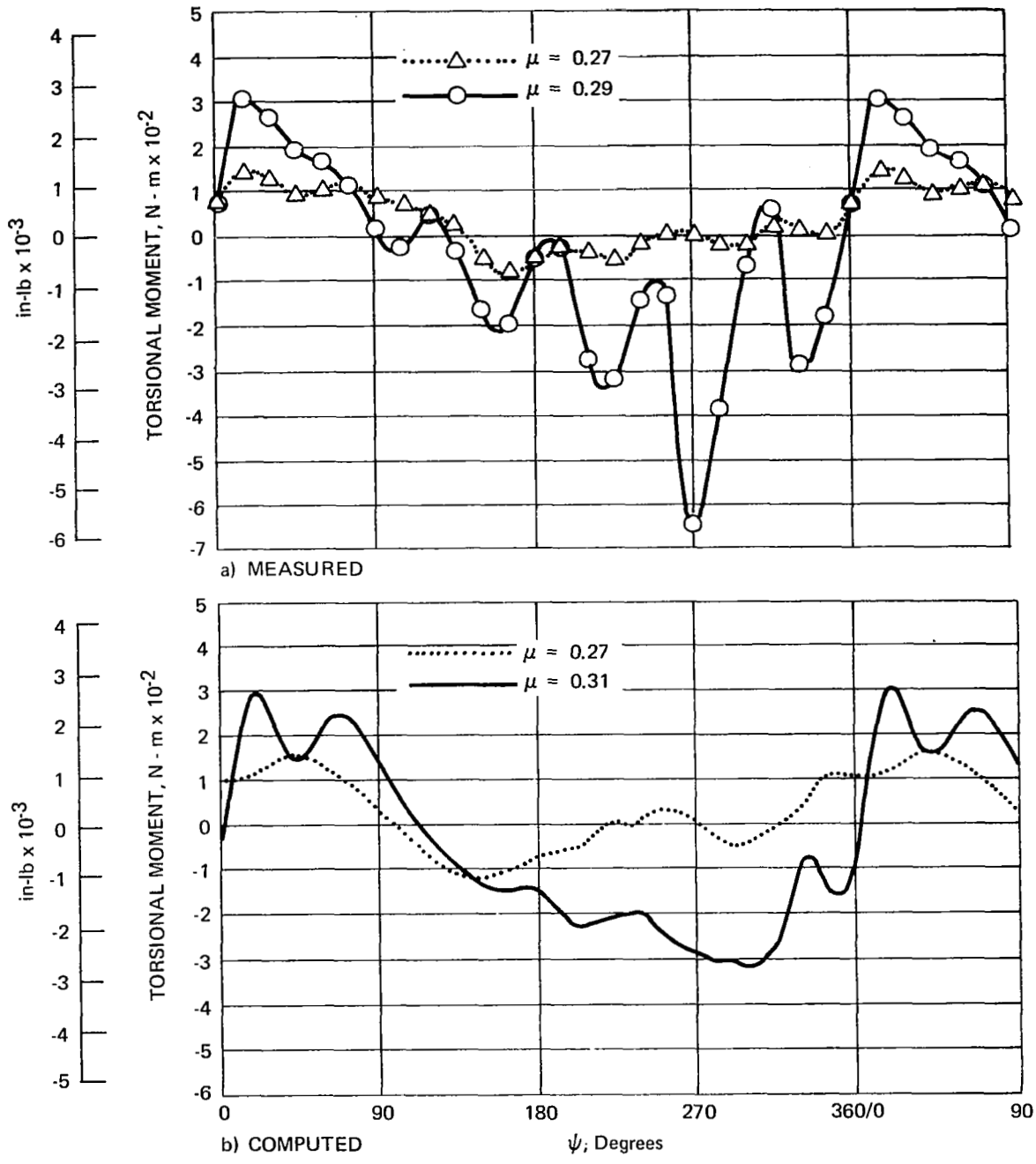

Figure 11 COMPARISON OF MEASURED AND COMPUTED H-34 BLADE TORSIONAL MOMENTS AT r/R = 0.15

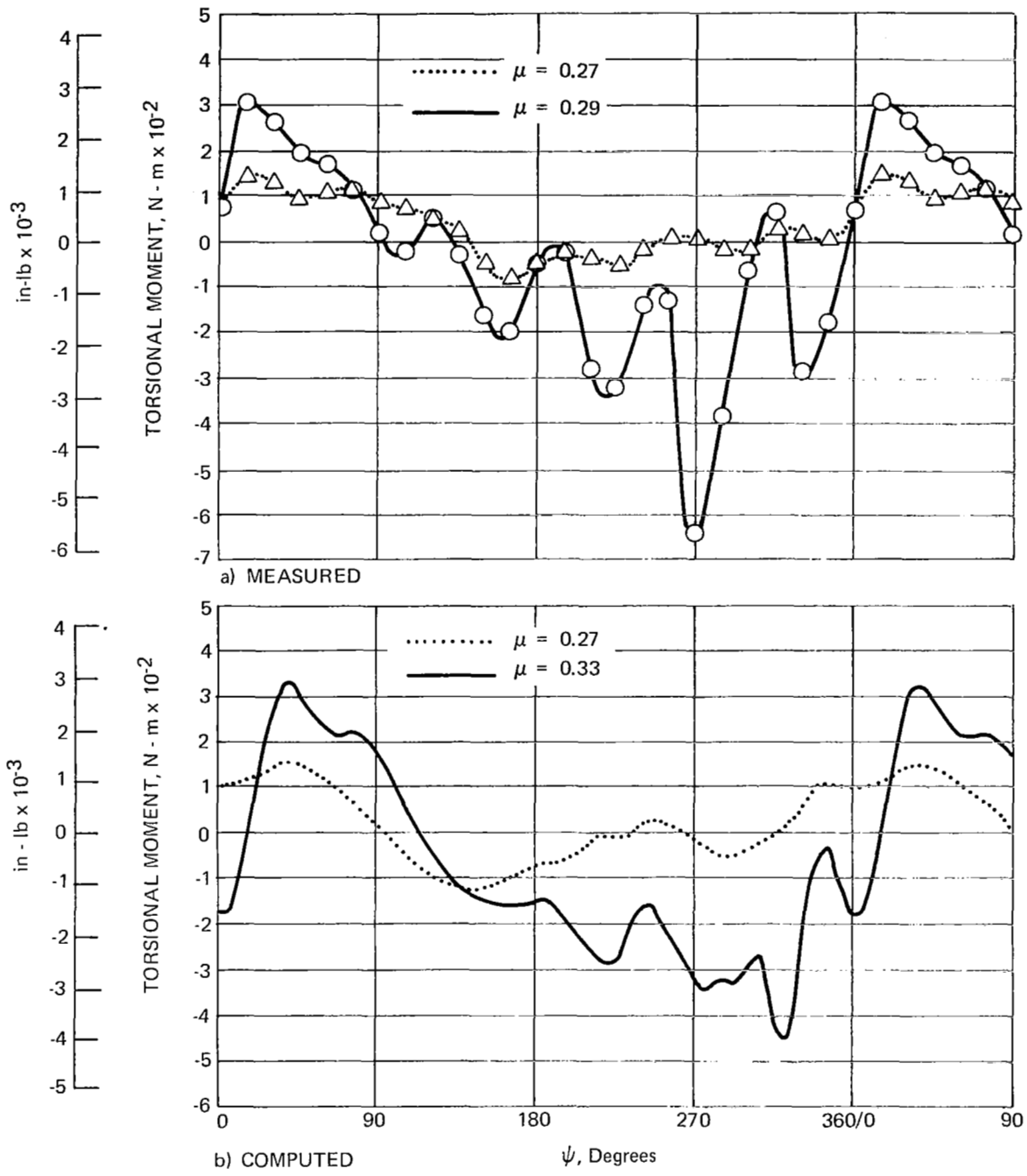

Figure 12 COMPARISON OF MEASURED AND COMPUTED H-34 BLADE TORSIONAL MOMENTS AT r/R = 0.15

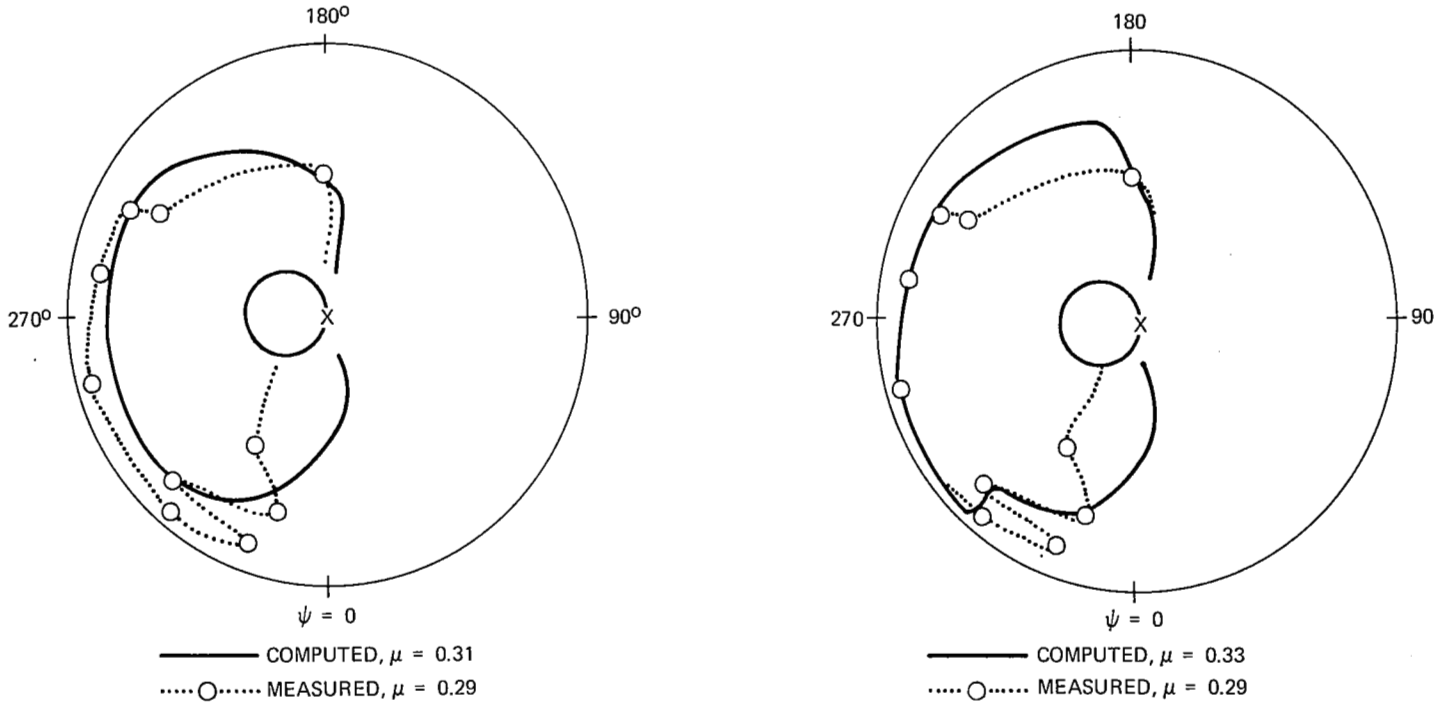

Figure 13 COMPARISONS OF COMPUTED AND MEASURED STALL ZONES

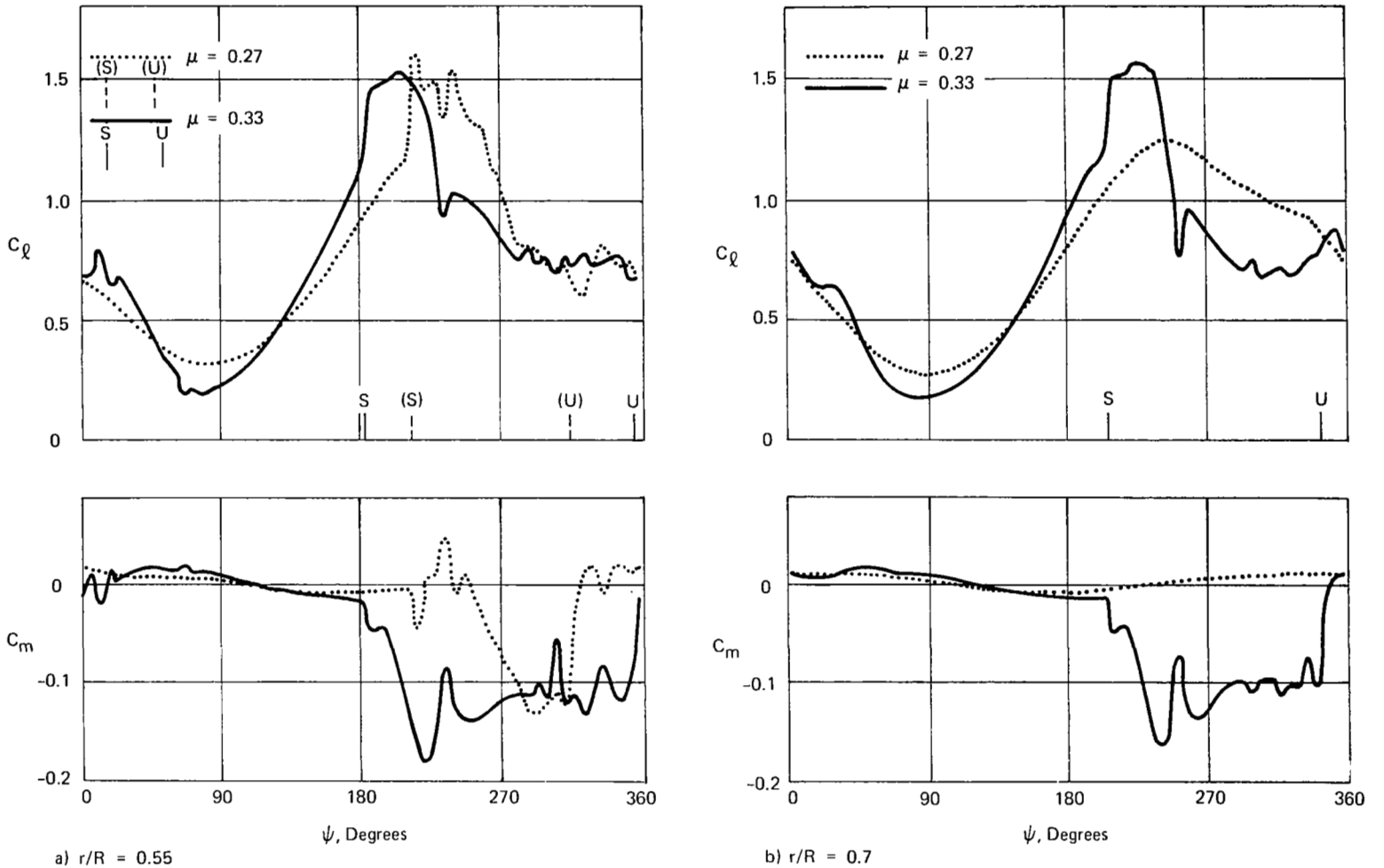

Figure 14 COMPUTED VARIATIONS OF H-34 BLADE SECTION LIFT AND MOMENT COEFFICIENTS

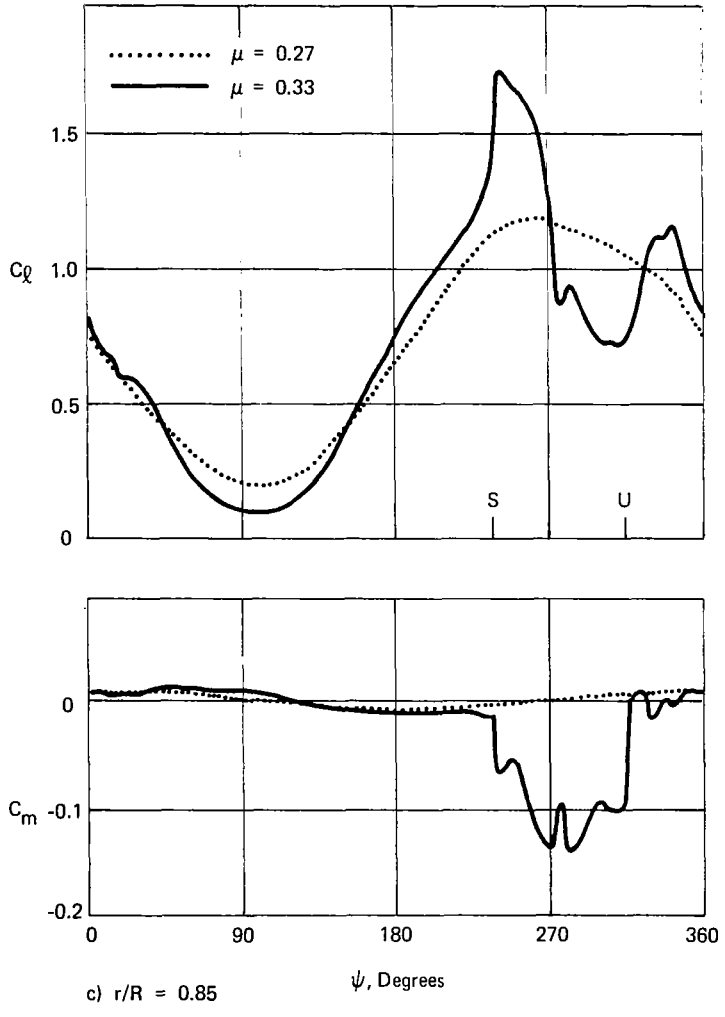

c) r/R = 0.85

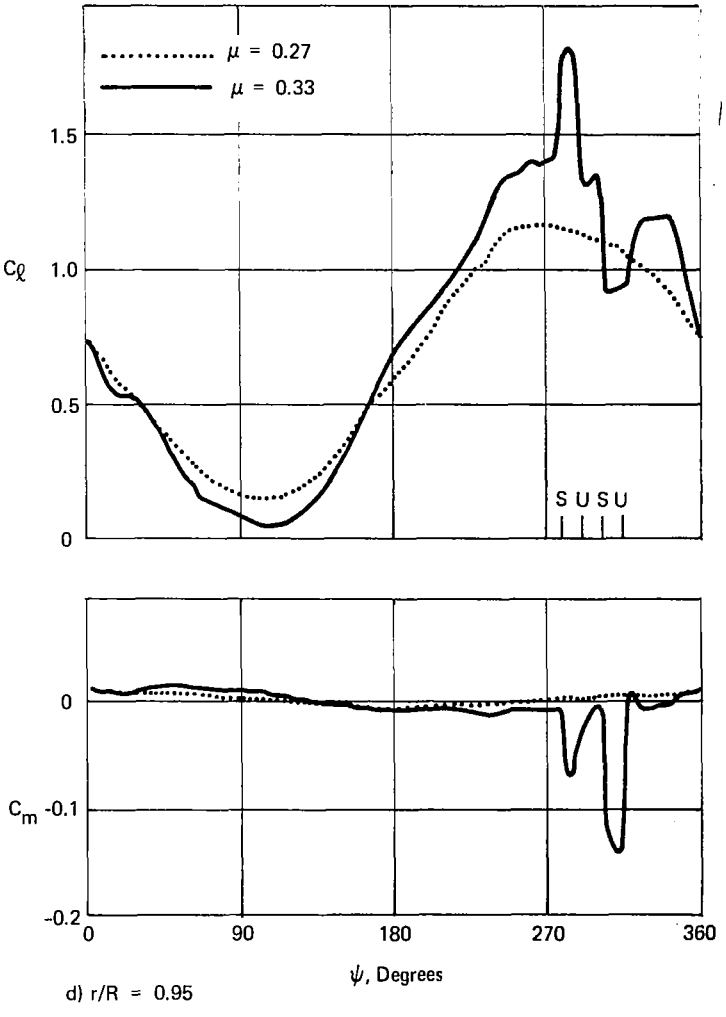

d) r/R = 0.95

Figure 14 (Concl'd)

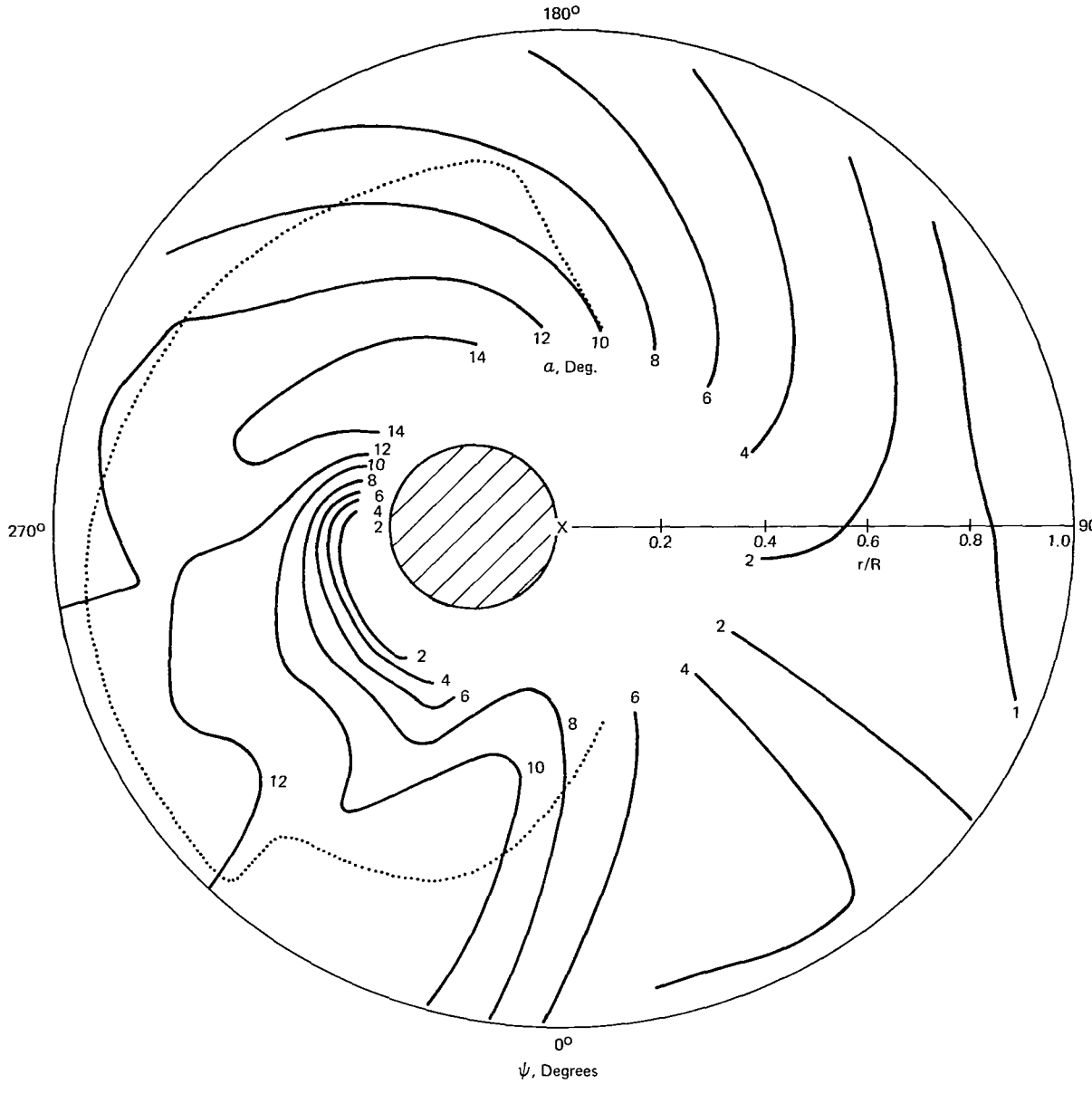

Figure 16 COMPUTED ANGLE OF ATTACK DISTRIBUTION AND STALL ZONE FOR $\mu = 0.33$

CH-54B. — It is reported in Ref. 12 that the CH-54B encountered stall-induced torsional oscillations during flight tests at a speed of 115 kts, or an advance ratio of .29. Analysis of the CH-54B at that advance ratio produced stall out to a radius of .7 R, but there was no appreciable torsional oscillation. Increasing the advance ratio to .33 caused an additional 15% of the blade to stall, which resulted in excessive torsional oscillations.

The computed pushrod load variations with ψ for the two advance ratios are shown in Fig. 17. The measured variation given in Ref. 12 is plotted without an ordinate scale, so a direct comparison is difficult. The measured oscillations are somewhat more severe than the computed ones, however. The former give a variation from maximum to minimum of about 4200 lbs, while the corresponding variation from the analysis is 2300 lbs. Also, the measured oscillations persisted through the first quadrant of the rotor plane, while they are confined to the fourth quadrant in the computed result.

The computed section lift and moment coefficients are plotted in Fig. 18 for four radial locations. The variations with ψ are seen to be quite similar to those obtained for the H-34. Stall progresses from root to tip, and again, a small increase in the extent of stall produced a large increase in the severity of torsional oscillations.

Effects of Variations in Torsion Frequency and Damping in Torsion

Other investigations have provided evidence that alterations in the blade vibrational characteristics can alleviate the problem of stall-induced torsional oscillations. Dampers were installed on the rotating control linkages of a CH-54B which reduced the 5th through 8th harmonics of the pushrod load by from 35% to 50% (Ref. 12). The analysis of Ref. 14 shows a reduction of about 40% in pitch-link loads would result by reducing the torsional frequency from $7\,\Omega$ to $5.5\,\Omega$. The H-34 rotor blade was analyzed, parametrically varying torsional frequency and introducing damping in torsion, to determine whether these effects could be detected.

The analysis of the H-34 with $\mu = .33$ was used as a basis for comparison. Torsion frequency was changed by adjusting the control stiffness. Viscous damping was introduced at two tenths of critical, which is the same amount as was produced by the control-linkage dampers of Ref. 12. The damping was assumed to act without altering the undamped torsional mode shape. The blade root torsional moment for each case was harmonically analyzed, obtaining the zeroth through ninth harmonics of the rotational frequency to provide a quantitative basis for comparison.

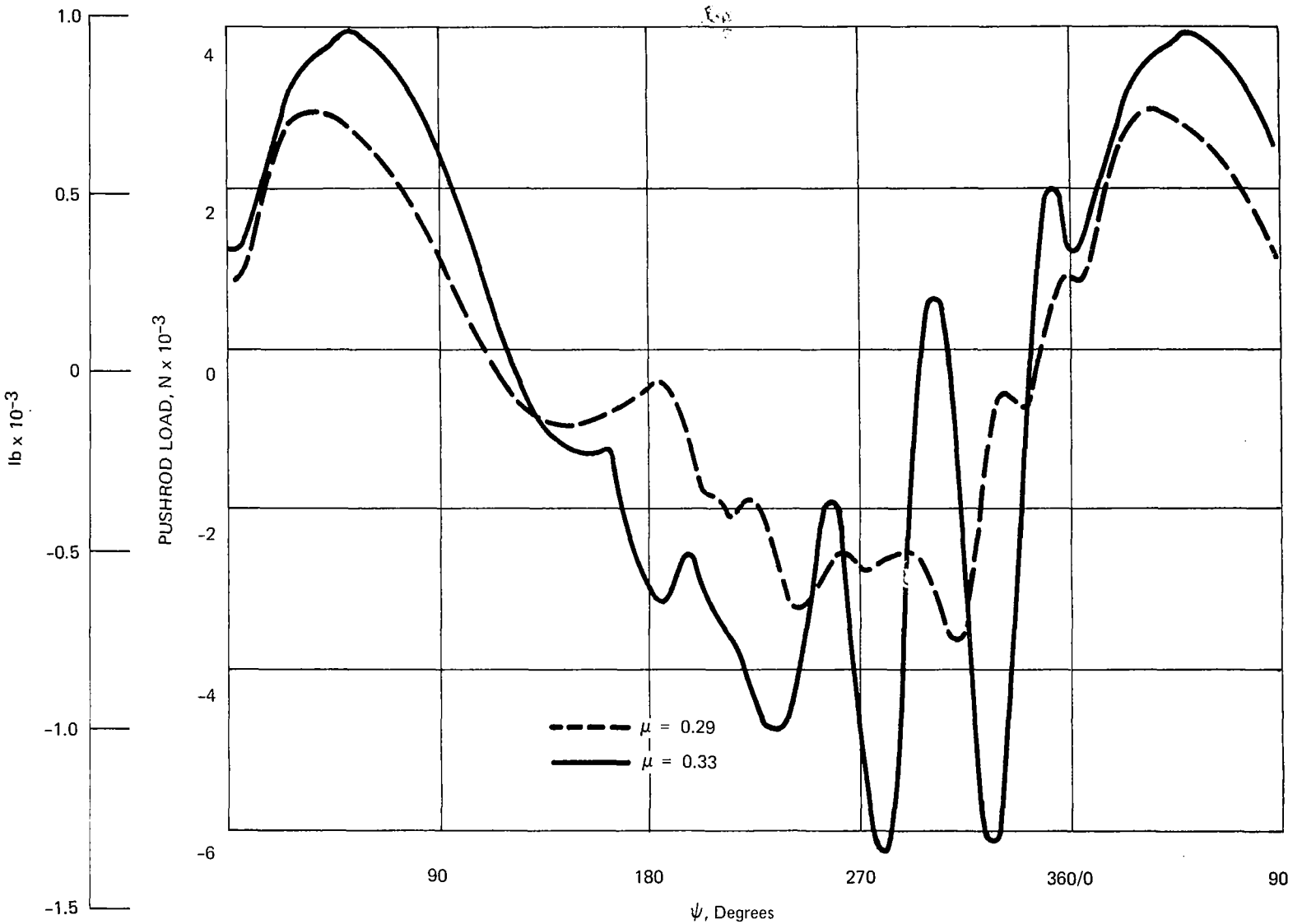

Figure 17 COMPUTED CH-54B PUSHROD LOADS

The effect of varying torsional natural frequency is shown in Fig. 19, which compares the amplitudes of the zeroth through ninth harmonics of the torsional moment for torsional natural frequencies (rotating) of 5.6 Ω , 6.6 Ω , and 7.6 Ω . Little effect is seen through the fourth harmonic. Increasing the frequency to 7.6 Ω lowered the fifth harmonic by 30%, but raised the sixth about the same amount and left the seventh through ninth nearly unchanged. Lowering the frequency to 5.6 Ω caused about a 30% increase in the fifth harmonic, but significantly lowered the sixth, seventh, and eighth. The largest of these, the seventh, was reduced by 60%. Lowering the torsional natural frequency does have a significant favorable effect, then, in agreement with what was found in Ref. 14.

The results of the harmonic analyses of the torsional moment for the three frequencies with and without damping in torsion are shown in Figs. 20, 21, and 22. Damping caused significant reductions for all three frequencies, and particularly so for a frequency of 6.6 Ω (Fig. 21). At that frequency, the seventh through ninth harmonics are reduced to almost negligible levels, and the zeroth, first and second are substantially reduced as well. The first harmonic, which is the largest, was reduced by 26%. These results indicate, then, that the introduction of damping in torsion can significantly reduce stall-induced torsional oscillations, which is in concurrence with the findings of Ref. 12.

Investigation of Boundary Layer Control

A preliminary study of the effectiveness and feasibility of using boundary layer control to reduce stall-induced torsional oscillations was conducted. To determine effectiveness, stall was not allowed to occur over a specified blade segment during the analysis of blade loading and response. Estimates were then made of pumping rates and power requirements, using available experimental data as a basis.

The H-34 rotor blade at an advance ratio of .33 was again analyzed. The procedure for evaluating the spanwise loading distribution was altered to account for boundary layer control, as follows. If the segment of blade designated to be controlled extends from $r = r_A$ to $r = r_B$, then three of the six radial points chosen for evaluating section loading were r_A, r_B, and the midpoint of the controlled segment, $r_c = (r_A + r_B)/2$. It was assumed that the loading on the controlled segment was constant and equal to its value at $r = r_c$. Spanwise integrations were then divided into three parts, one from the blade root to r_A, another from r_A to r_B, and the third from r_B to the tip, in order to allow for the possible loading discontinuities at r_A and/or r_B. Stall was not allowed to occur at $r = r_c$, but the leading-edge bubble was still analyzed there. The results of those analyses were used in

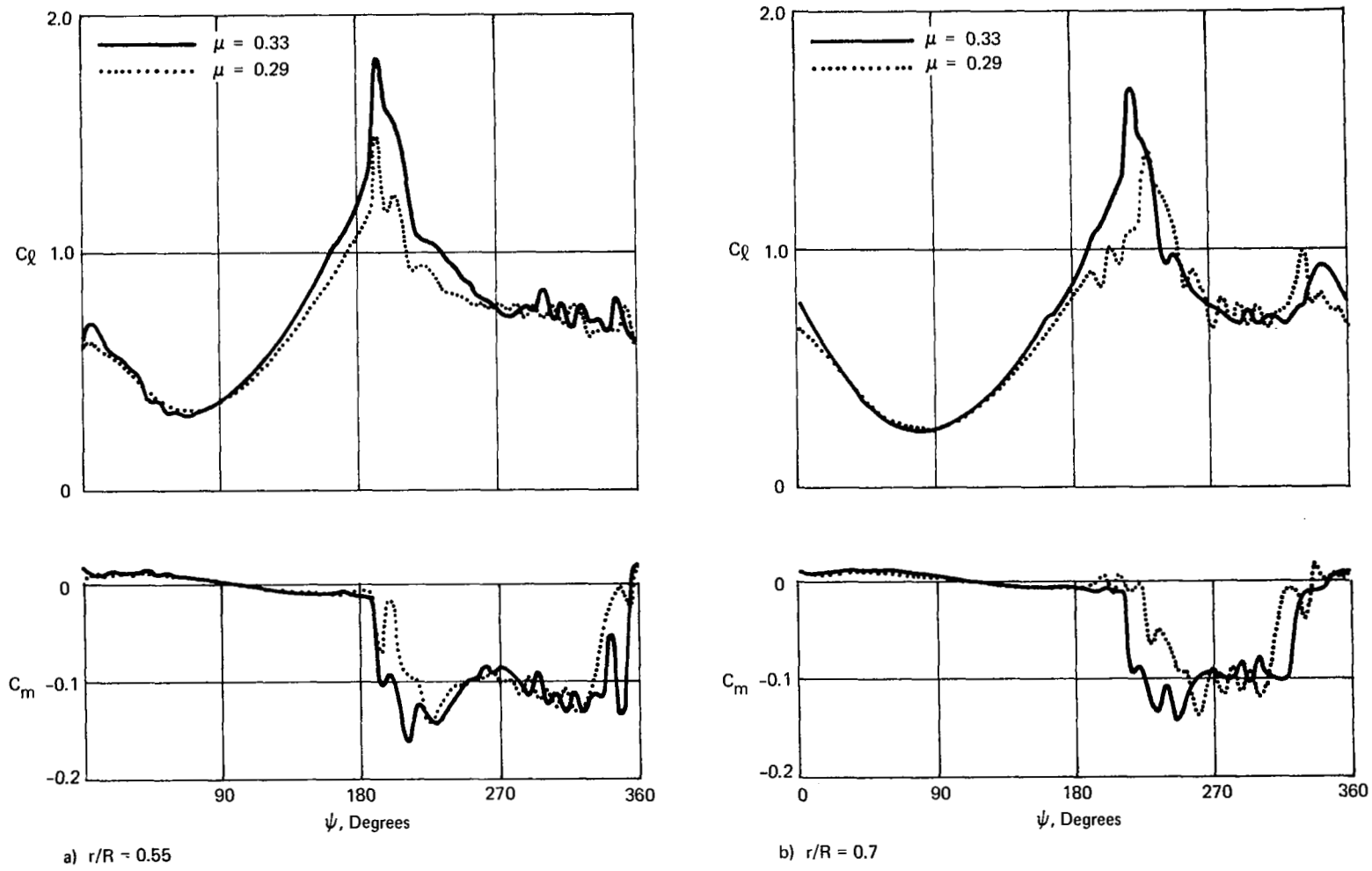

Figure 18 COMPUTED VARIATIONS OF CH-54B BLADE SECTION LIFT AND MOMENT COEFFICIENTS

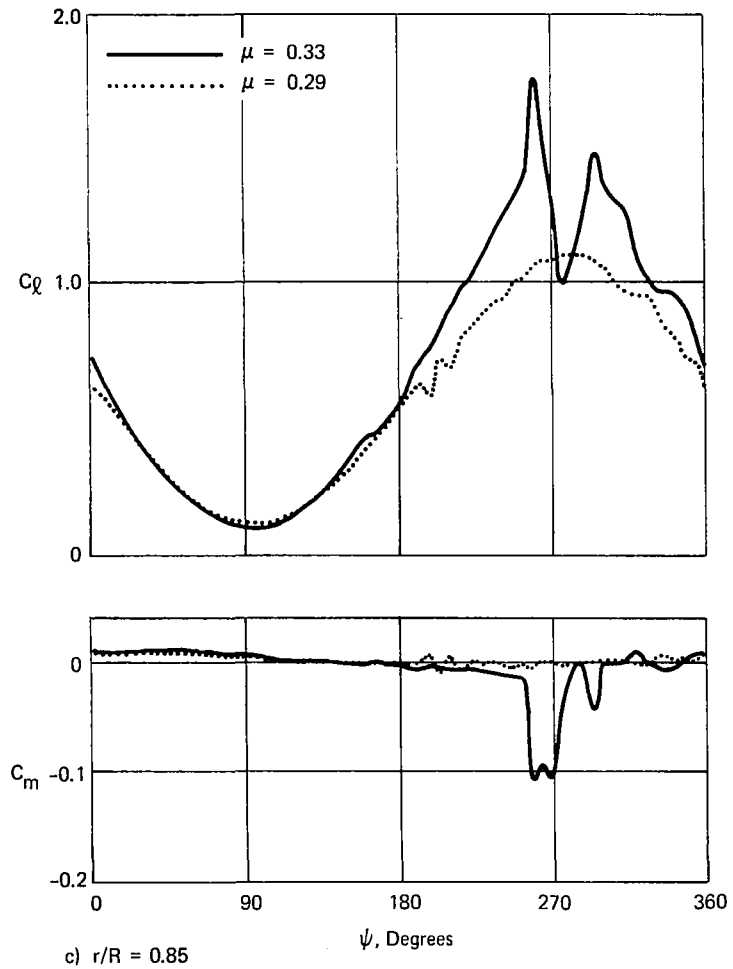

c) r/R = 0.85

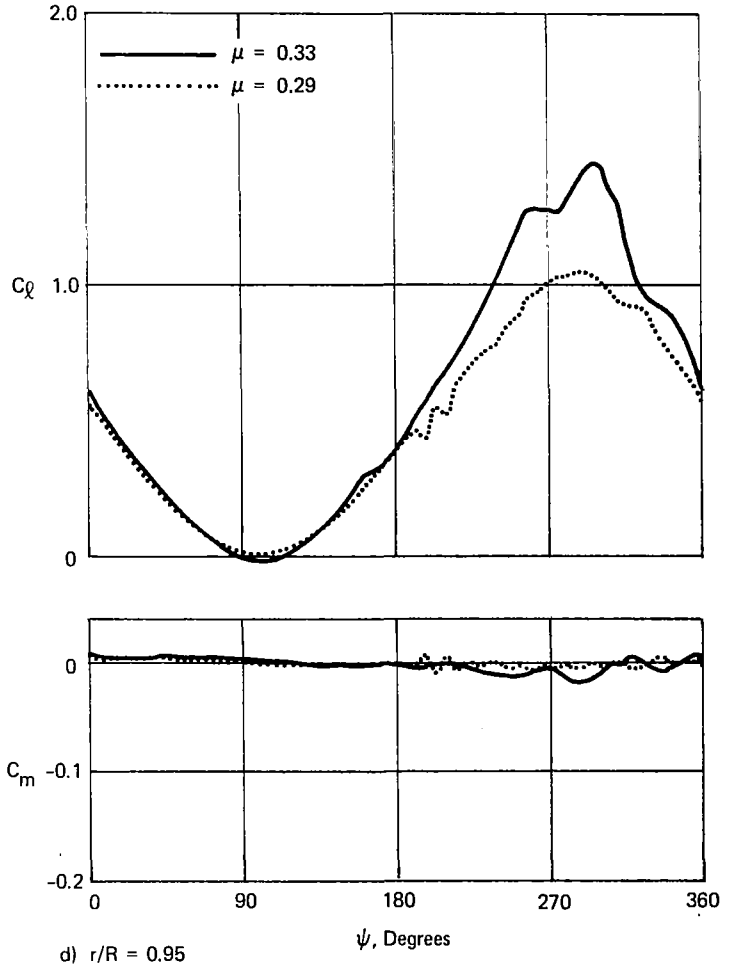

d) r/R = 0.95

Figure 18 (Concl'd)

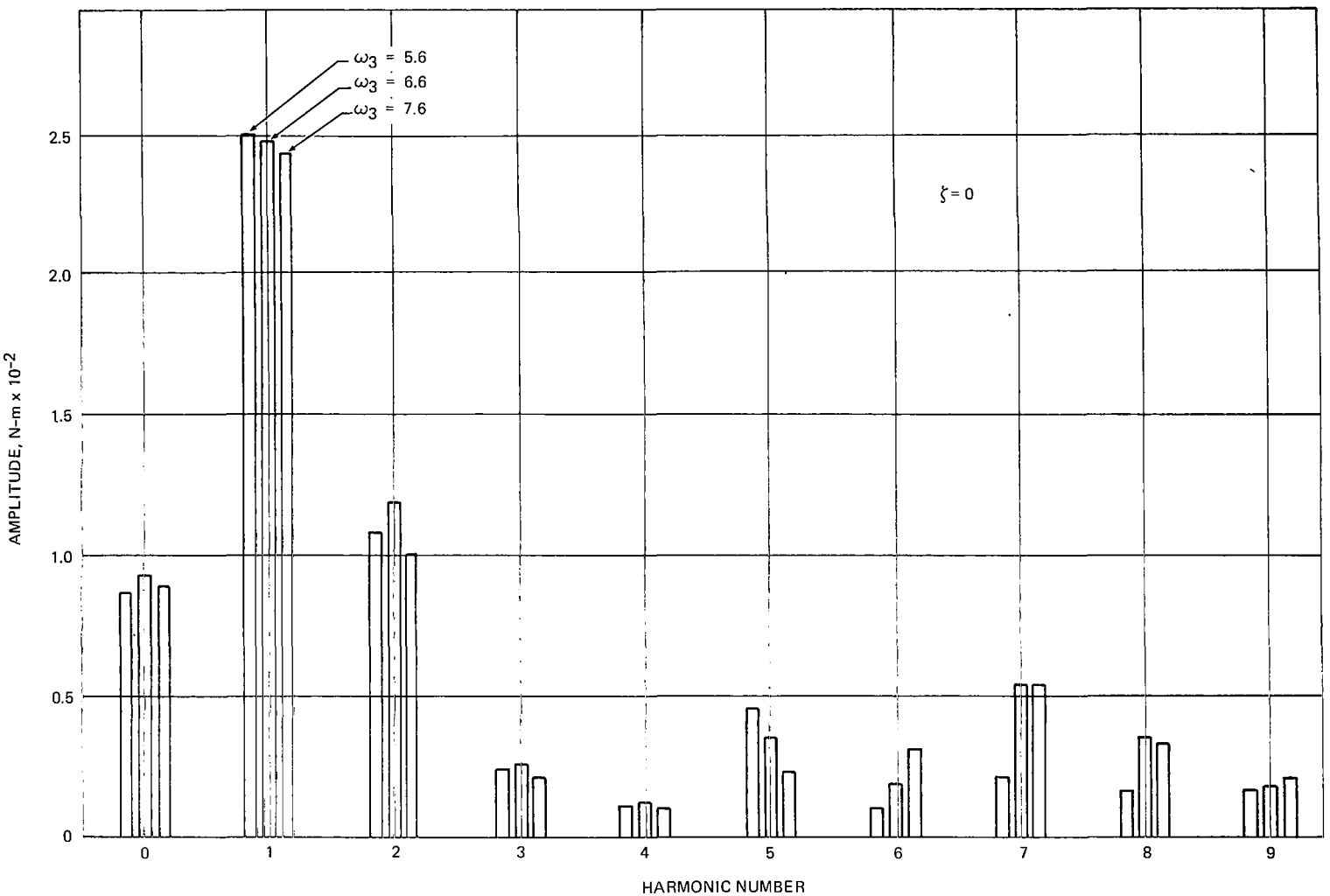

Figure 19 EFFECT OF TORSION FREQUENCY ON TORSIONAL MOMENT HARMONIC COMPONENTS

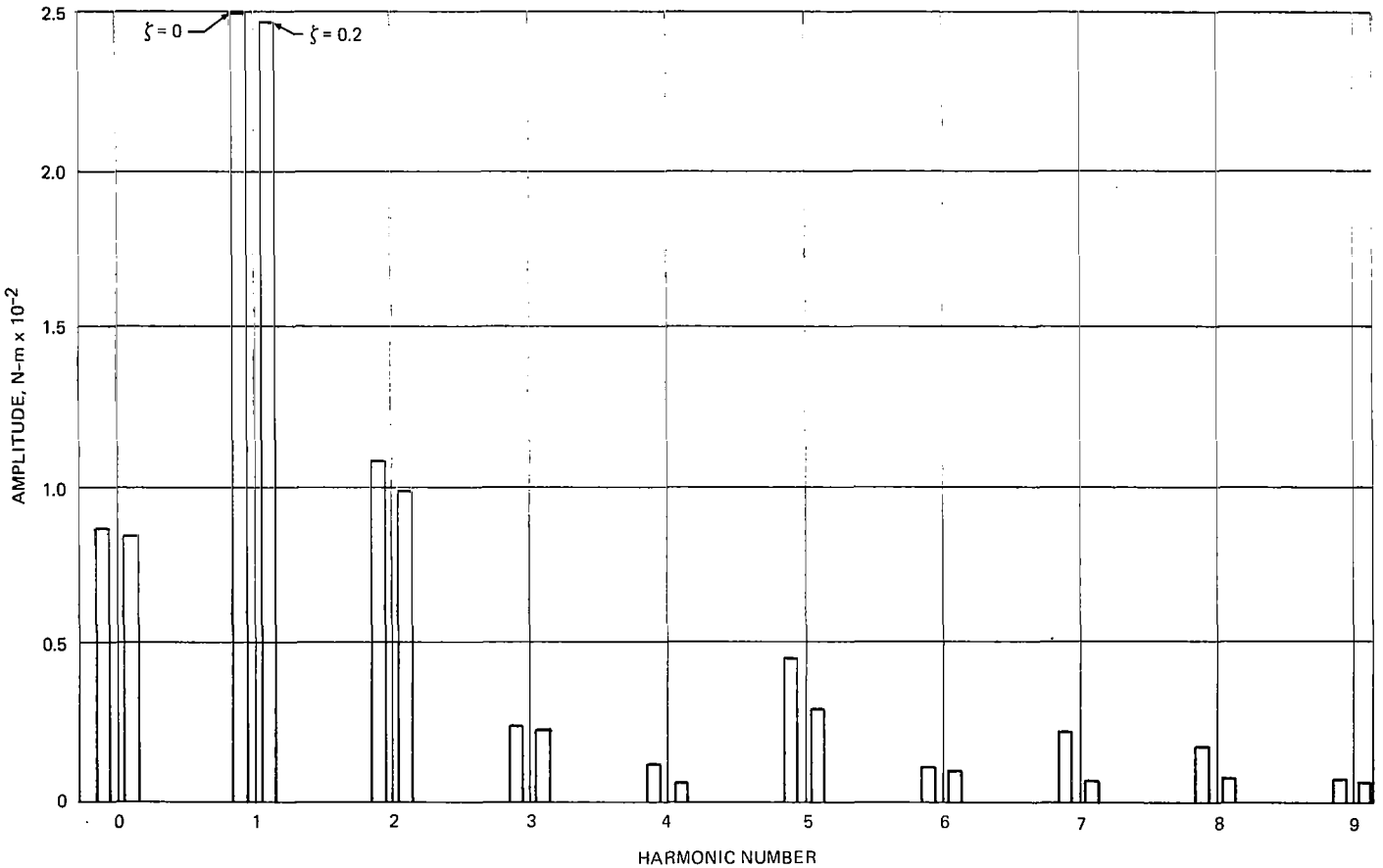

Figure 20 EFFECT OF DAMPING ON TORSIONAL MOMENT HARMONIC COMPONENTS, ω_3 = 5.6

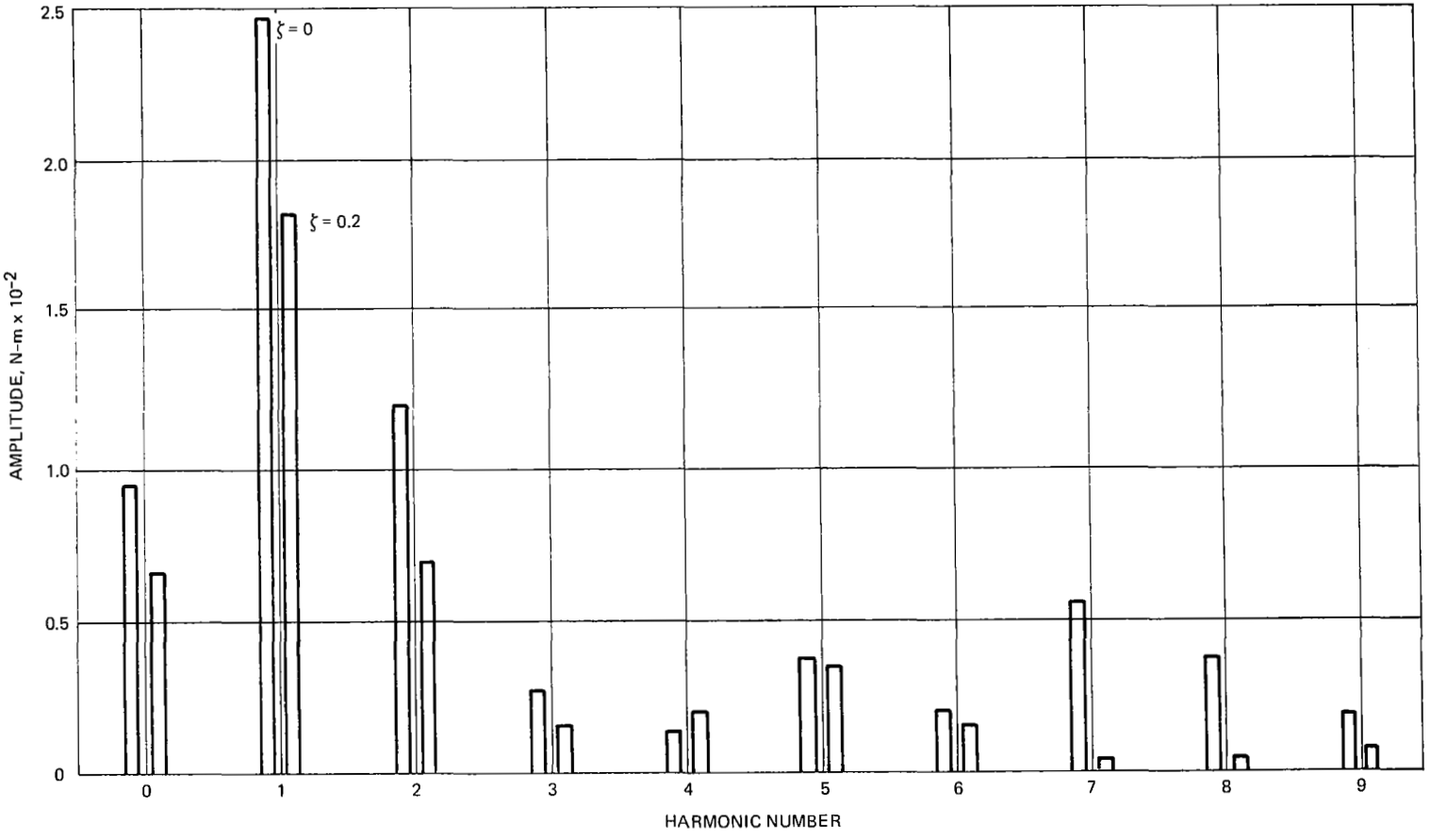

Figure 21 EFFECT OF DAMPING ON TORSIONAL MOMENT HARMONIC COMPONENTS, $\omega_3 = 6.6$

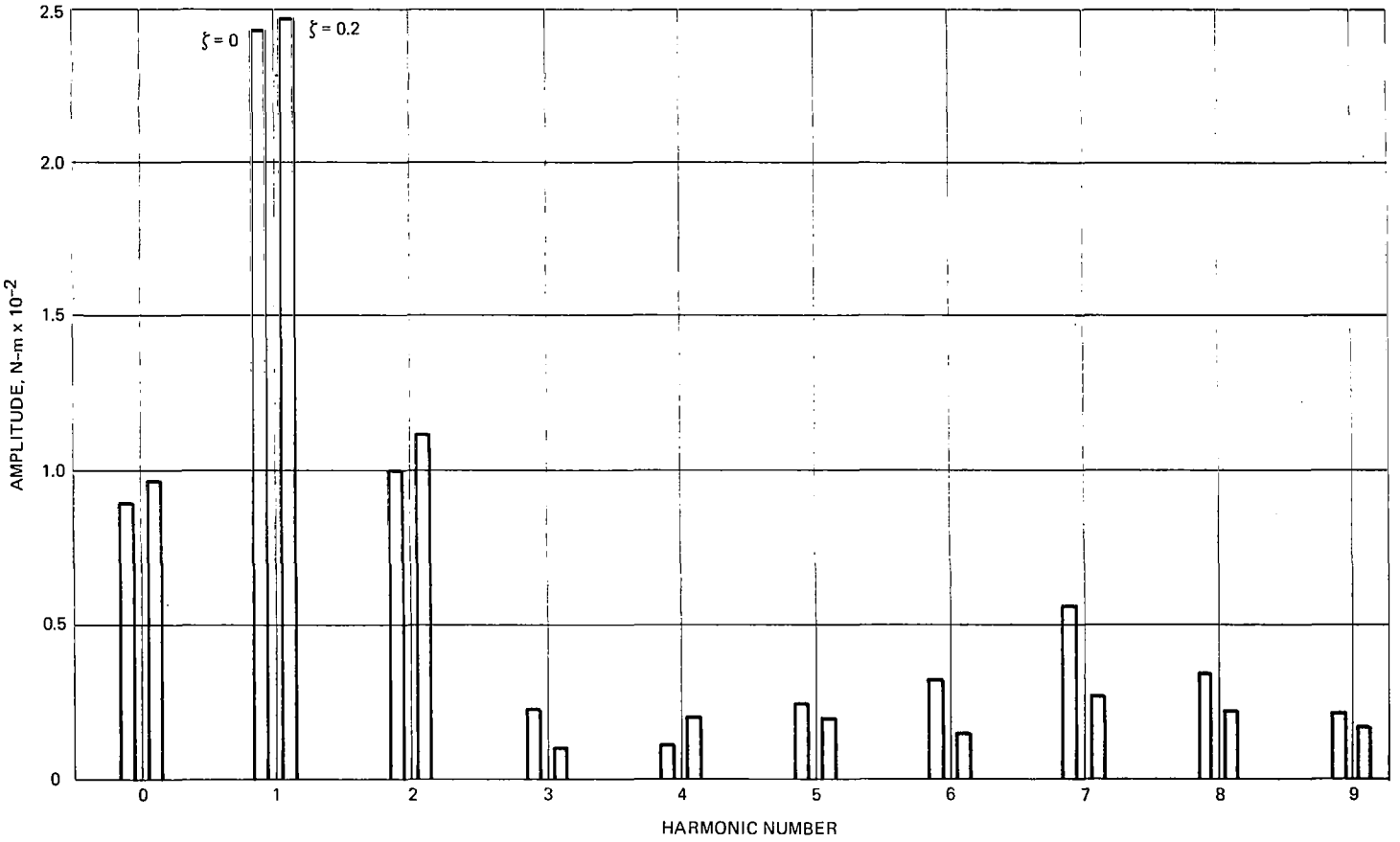

Figure 22 EFFECT OF DAMPING ON TORSIONAL MOMENT HARMONIC COMPONENTS, $\omega_3 = 7.6$

the estimates of pumping and power requirements. The blade root torsional moments were again harmonically analyzed for comparison with the case of no boundary layer control.

The blade was analyzed for lengths of the controlled segment of blade, l_c, of .05 R, .1 R, and .15 R. The results are presented in Figs. 23, 24, and 25, where the amplitudes of the fifth through eighth harmonics of the torsional moment are compared for different values of r_c. The lower harmonics were generally reduced by boundary layer control, but the reductions are not substantial and no clear trends are evident, so only the higher harmonics are shown.

As one would expect, increasing l_c reduces the severity of the torsional oscillations. For l_c of .1 R and .15 R (Figs. 24 and 25), it is apparent, as well, that control near the tip is more effective than control over an inboard section. The greatest overall reduction in the amplitudes of the higher harmonics was obtained with l_c = .15 R and r_c = .9 R, with the largest of these, the seventh, reduced by 95%. The variation of the torsional moment with ψ for that case is compared with the result for no control in Fig. 26.

In order to estimate pumping and power requirements, data were used from the wind tunnel tests on an airfoil with 9% thickness ratio at a Reynolds number of 1.15×10^6 reported in Ref. 20. Boundary layer control in those tests was effected by suction over a surface area near the leading edge comprising 2.75% of chord. The results are summarized in Fig. 27, taken from Ref. 20, which shows the lift coefficient vs. incidence for various suction rates. The suction rate required to just prevent stall is seen to increase approximately linearly with incidence, with a value for $C_Q \sqrt{Re}$ of 3.61 being sufficient to increase the stall angle from 10 degrees to 16 degrees; the suction coefficient $C_Q = Q/(Uc)$, Q being the volume flow per unit span and U the free-stream speed. The product $C_Q \sqrt{Re}$ is used because results are nearly independent of Re for a given value of that parameter.

In order to compute Q from these results, the equivalent of airfoil static angle of attack is needed. As is apparent from the results presented previously, the actual angle of incidence is not a good measure of how far the airfoil is above the stall condition in unsteady flow, so results from the analysis of the leading-edge bubble were used. Let Δ_r denote the required increase in pressure coefficient across the bubble, and Δ_p the increase which is possible, as defined in Ref. 8. Then, a parameter ξ_c is defined by

$$\xi_c = \left[\frac{\Delta_r - \Delta_p}{\Delta_r}\right]^{1/2}, \quad \Delta_r \geq \Delta_p ;$$

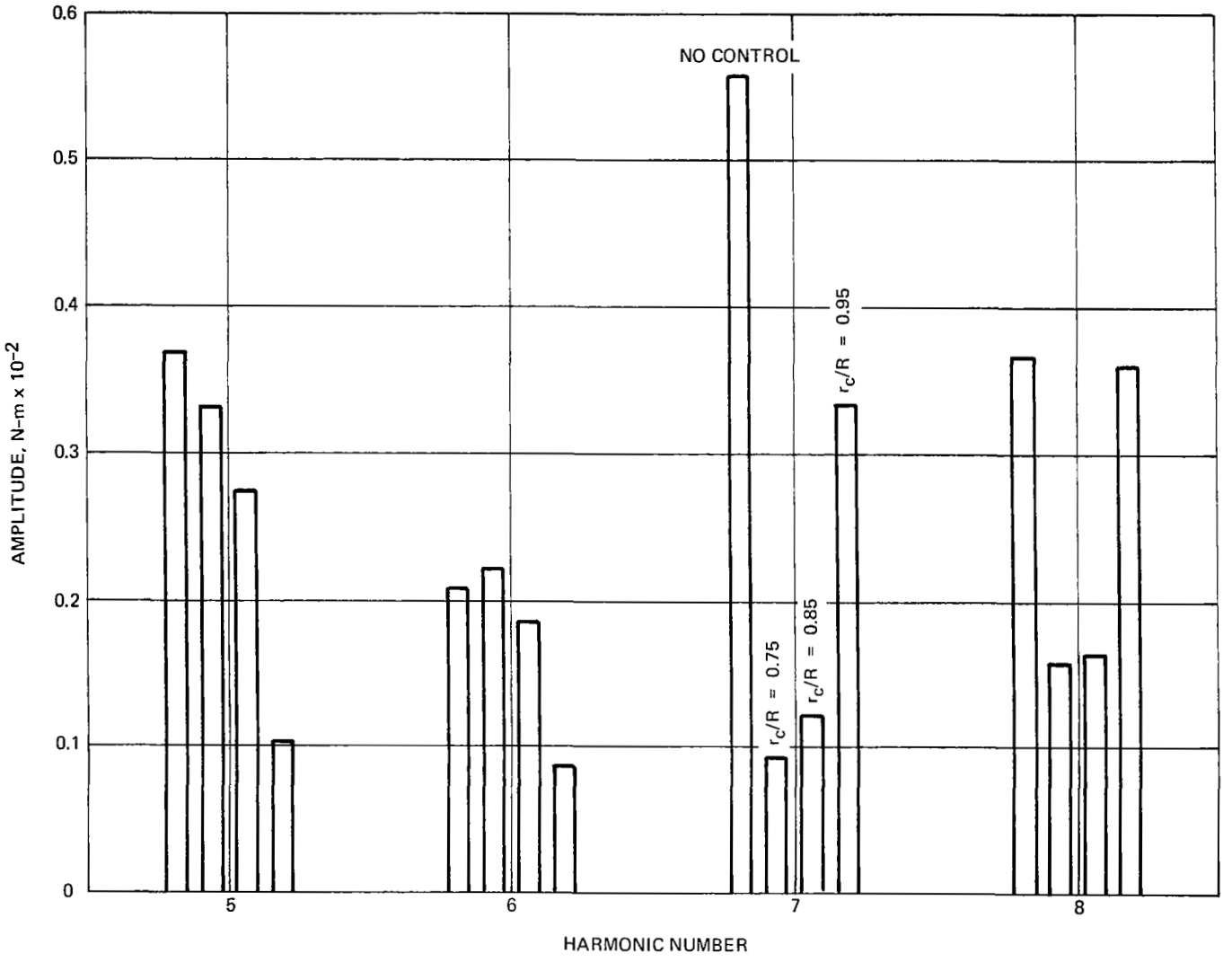

Figure 23 HIGHER HARMONICS OF TORSIONAL MOMENT WITH ℓ_c/R = 0.05

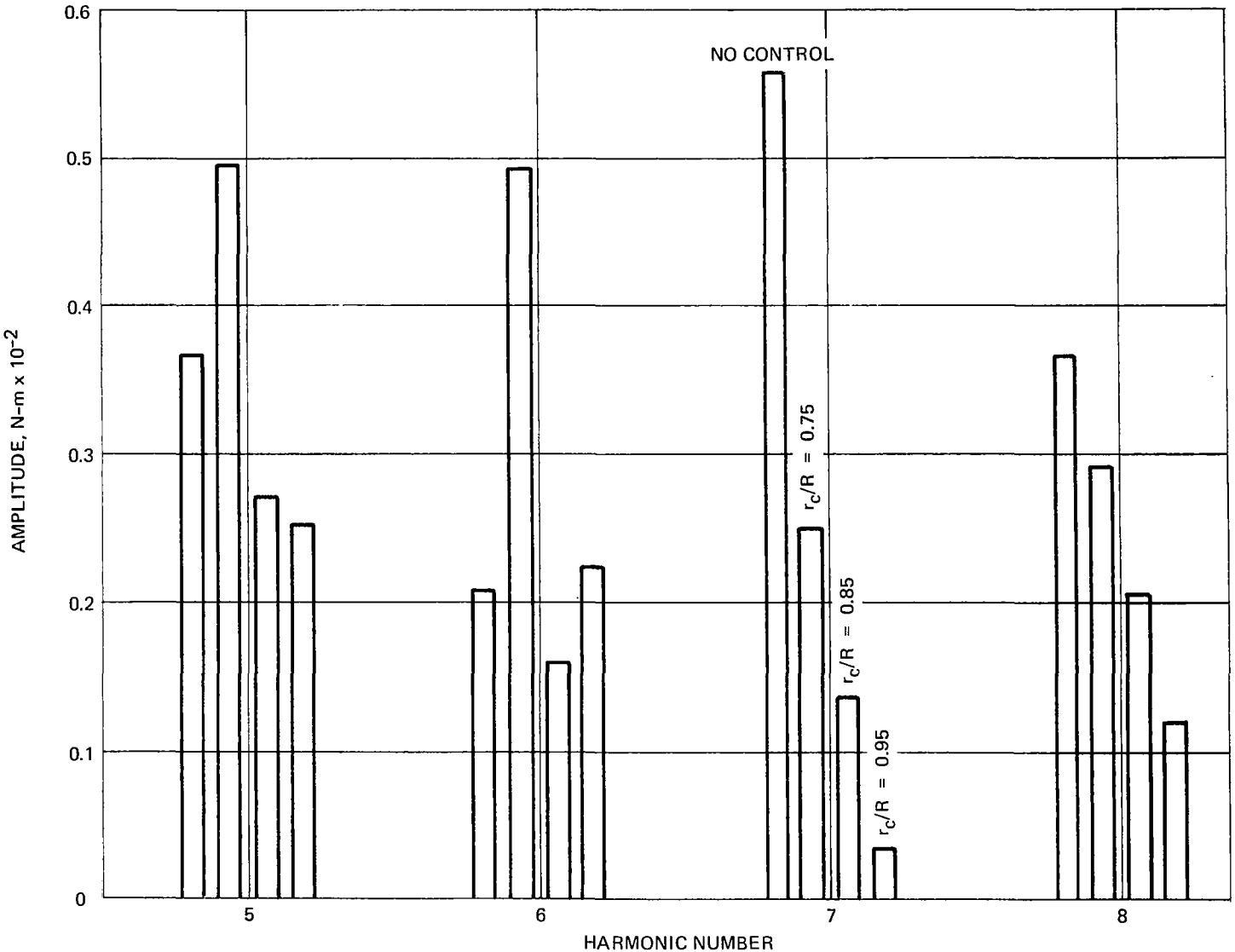

Figure 24 HIGHER HARMONICS OF TORSIONAL MOMENT WITH $\ell_c/R = 0.1$

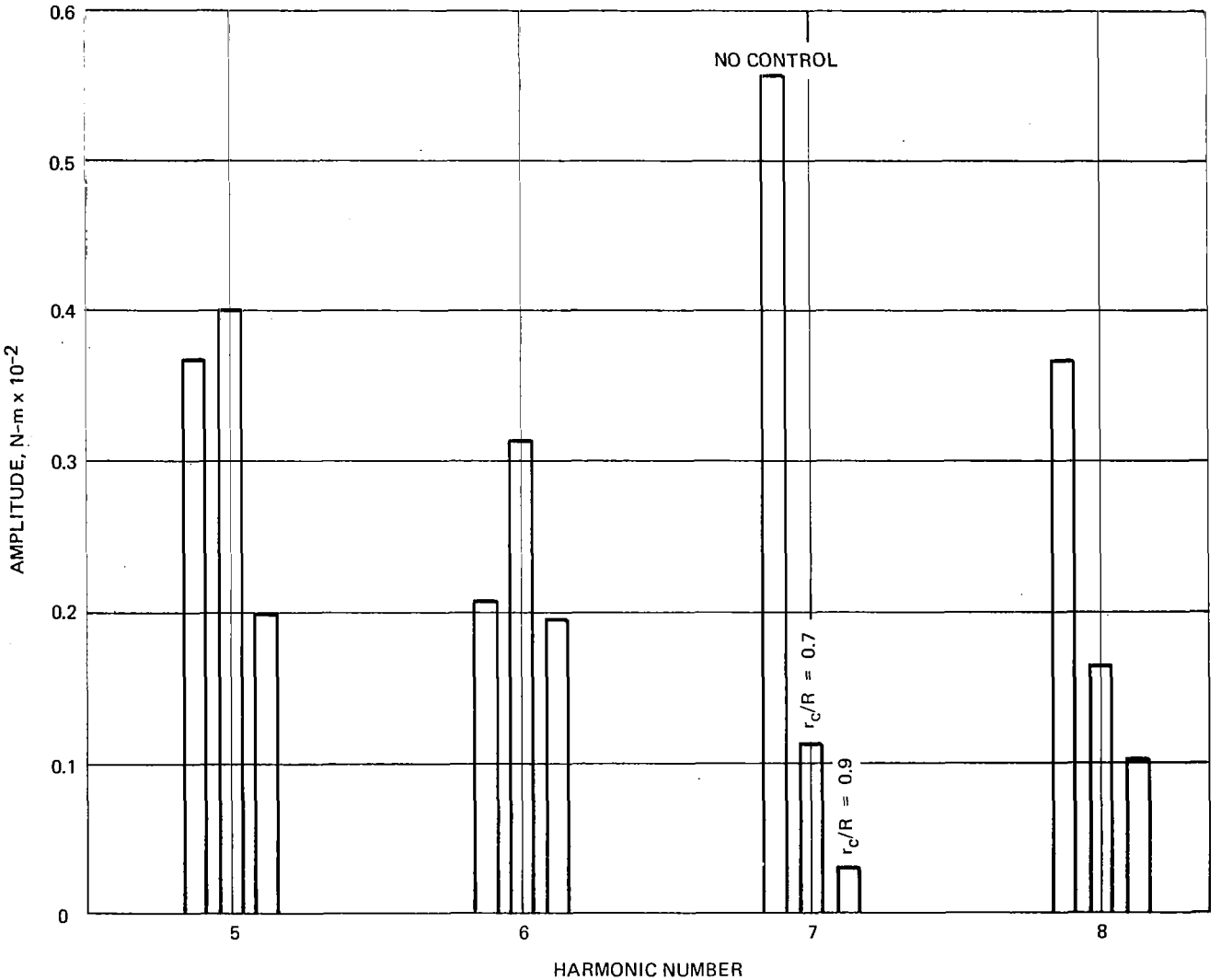

Figure 25 HIGHER HARMONICS OF TORSIONAL MOMENT WITH ℓ_c/R = 0.15

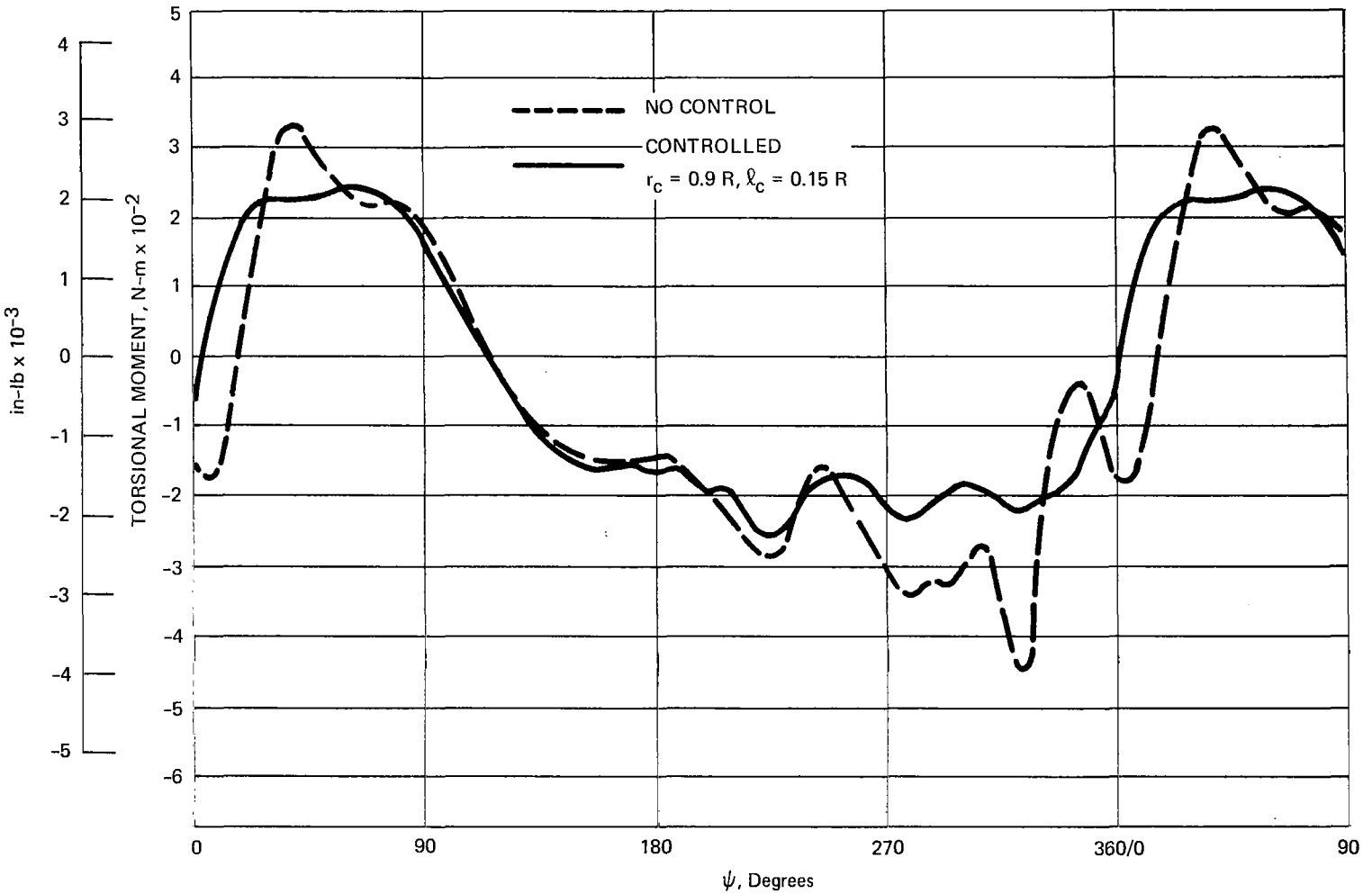

Figure 26 VARIATIONS OF BLADE ROOT TORSIONAL MOMENT WITH AND WITHOUT BOUNDARY LAYER CONTROL

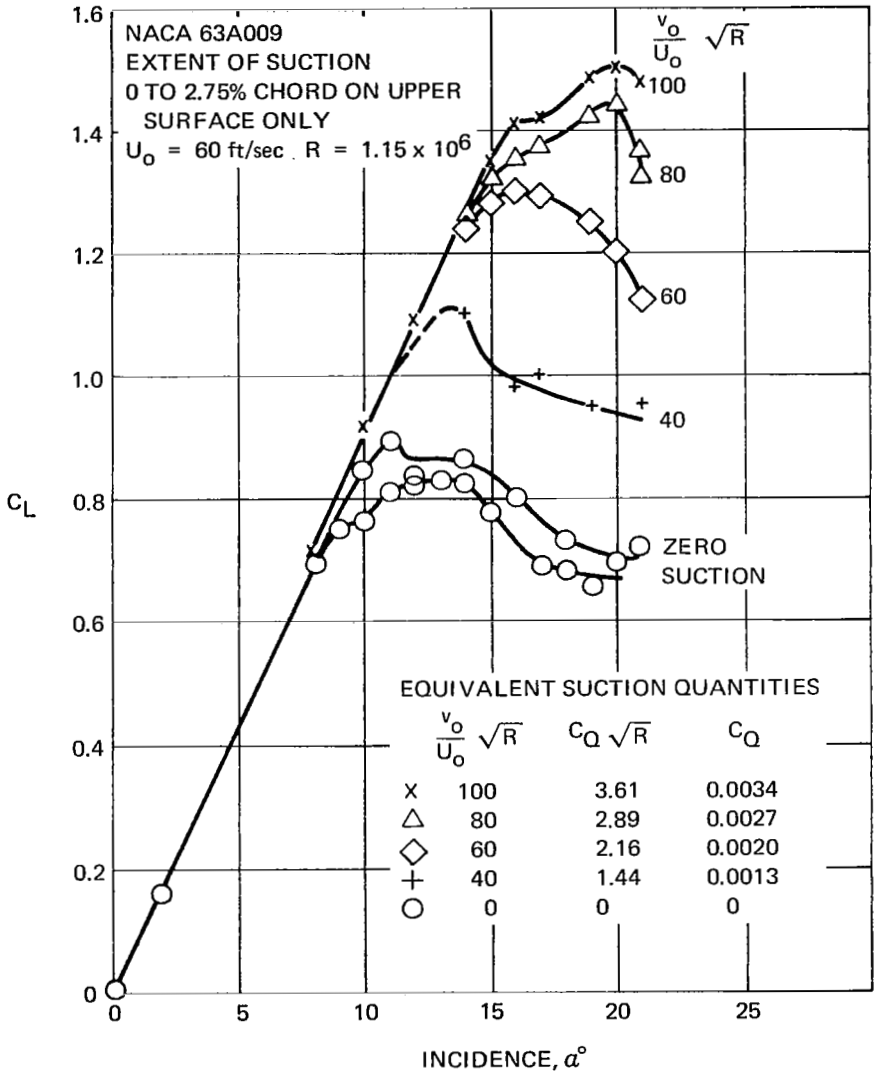

Figure 27 VARIATION OF LIFT COEFFICIENT WITH INCIDENCE AND SUCTION QUANTITY (FIG. 9 OF REF. 20)

to provide a measure of how far above stall an airfoil is under either steady or unsteady conditions. To relate ξ_c to static angle of attack, the leading-edge bubble was analyzed in steady flow with stall precluded for several angles of attack above the stall incidence, with the result shown in Fig. 28. The parameter ξ_c was defined so it would vary linearly with angle of attack near the static stall angle, as can be seen is the case from Fig. 28.

The data of Fig. 27 were combined with the results of Fig. 28 to give the plot of $C_Q\sqrt{Re}$ vs. ξ_c shown in Fig. 29. The maximum value of ξ_c at r_c for each run was determined and the corresponding value of $C_Q\sqrt{Re}$, taken from Fig. 29, was used to compute required suction rate.

The power required was computed as the product of the total volume flow per blade, Q_{TOT}, the increase in total pressure supplied by the pump, and the number of blades, N_B. Neglecting duct losses and assuming exhaust is to atmospheric pressure, the total required power is given by

$$P_s = \frac{1}{2} N_B Q_{TOT} \rho (q_s^2 + \Omega^2 r_c^2)$$

where q_s is the magnitude of fluid velocity at the edge of the boundary layer at separation.

Results are summarized in Table 2. Calculations for $r_c/R = .95$ and $l_c/R = .05$ could not be performed because Δ_r never exceeded Δ_p during the run but, as might be expected, the reduction in torsional response was not appreciable for that case (see Fig. 23). The suction rates and power required for all cases are relatively modest. It should be noted that requirements do not necessarily increase with effectiveness, since the case resulting in the most reduction in torsional oscillations ($r/R = .9$, $l_c/R = .15$) does not require the most power of the cases analyzed, by a considerable margin. In light of these results, the primary factor in determining whether boundary layer control is implemented would appear to be the mechanical complexity and resulting cost, rather than duct size or power requirements.

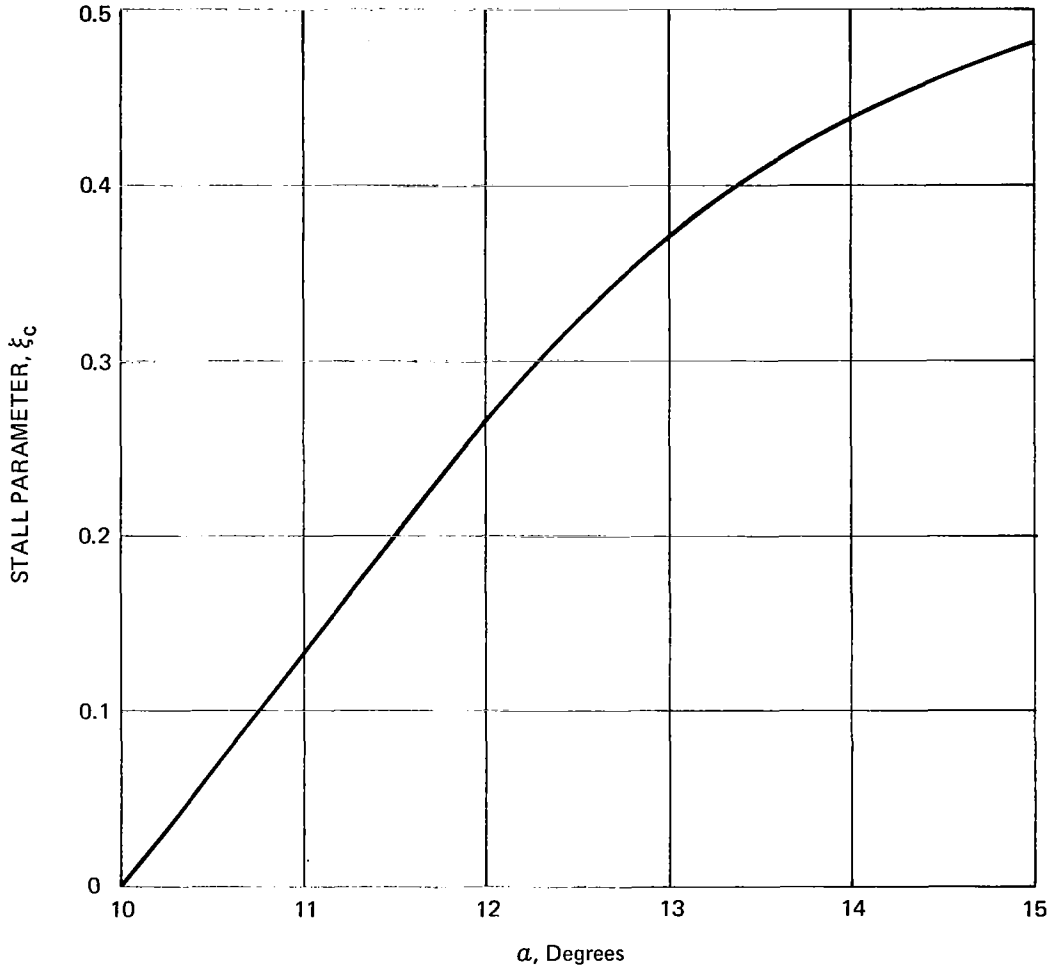

Figure 28 VARIATION OF STALL PARAMETER WITH STATIC ANGLE OF ATTACK

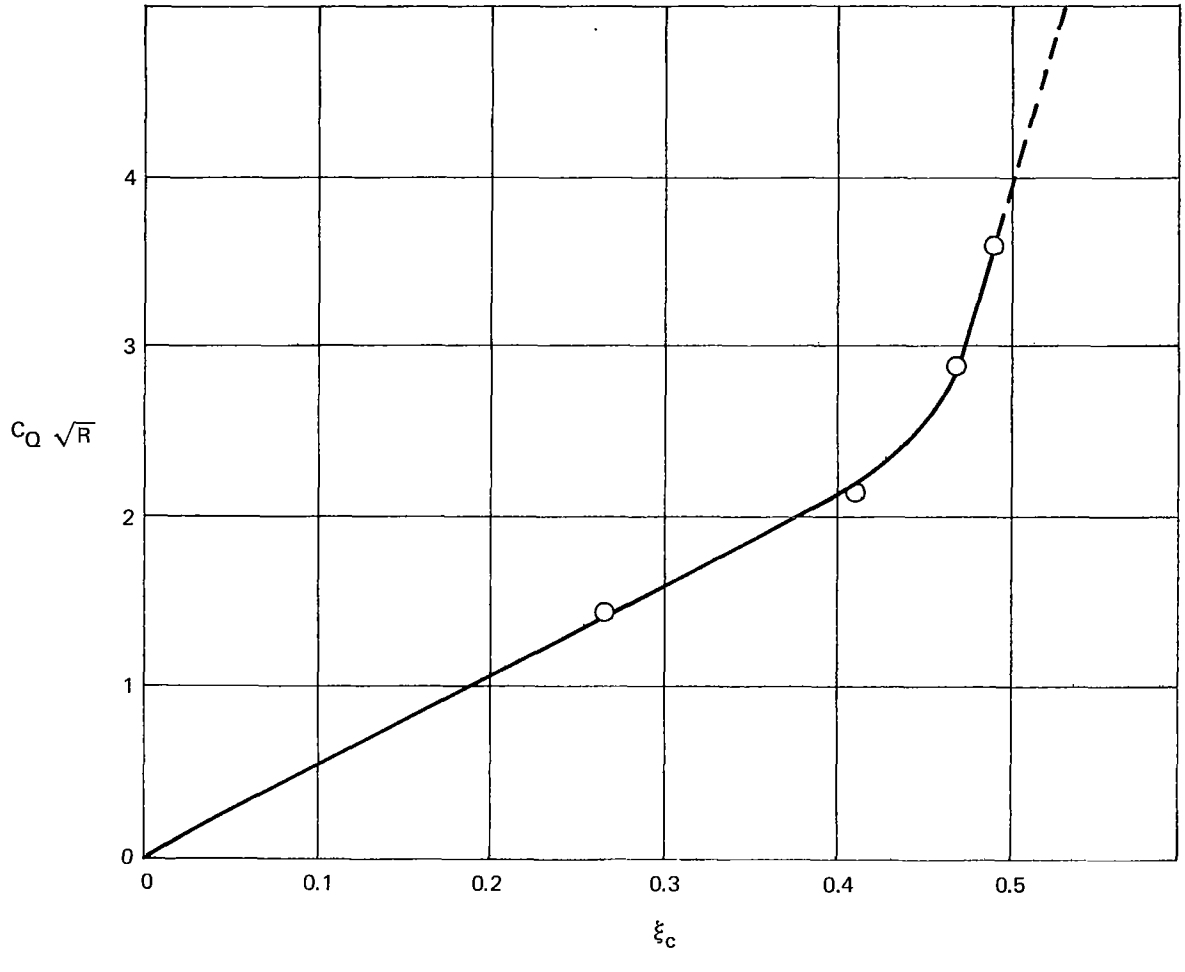

Figure 29 VARIATION OF SUCTION COEFFICIENT WITH STALL PARAMETER

TABLE 2

SUCTION RATE AND POWER REQUIREMENTS

r_c/R	l_c/R	$\xi_{c_{max}}$	$C_Q\sqrt{Re}$	$10^{-6}Re$	$q_s/(\Omega R)$	Q_{TOT} m^3/sec	P_s hp
.75	.05	.527	4.95	1.47	1.42	.0578	17.7
.85	.05	.405	2.18	1.84	1.65	.0286	11.7
.95	.05	--	--	--	--	--	--
.75	.10	.553	5.90	1.49	1.50	.139	46.5
.85	.10	.369	1.97	1.82	1.69	.0513	21.7
.95	.10	.233	1.25	2.23	1.99	.0360	20.7
.7	.15	.596	7.50	1.35	1.39	.252	72.3
.9	.15	.283	1.50	2.00	1.83	.0614	30.3

CONCLUSIONS

An analysis of helicopter rotor blade torsional oscillations due to stall has been carried out, using an analytic dynamic stall representation to determine aerodynamic loading. The following conclusions can be drawn from the results obtained.

1. The analytic representations employed will predict the torsional oscillations due to stall and their relationship to blade and flight parameters. In a comparison of data from flight tests with results of analyses, the severity of the oscillations and their relation to aircraft forward speed agreed fairly well, while the radial and azimuthal extents of stall and the azimuthal variations of section loading were in good agreement.

2. The amplitudes of the higher harmonics of torsional oscillations can be significantly reduced by either reducing the torsional natural frequency or introducing viscous damping in the torsional degree of freedom.

3. Boundary layer control would be an effective means for reducing the higher harmonics of torsional oscillations due to stall. Its implementation would not require excessive power or suction rates.

REFERENCES

1. Ham, N. D.; and Young, M. I.: Torsional Oscillation of Helicopter Blades Due to Stall. J. Aircraft, vol. 3, no. 3, May-June 1966, pp. 218-224.

2. Liiva, J.; et al.: Two-Dimensional Tests of Airfoils Oscillating Near Stall. USAAVLABS Tech. Rept. no. 68-13A, April 1968.

3. Martin, J. M.; Empey, W. J.; McCroskey, W. J.; and Caradonna, F. X.: An Experimental Analysis of Dynamic Stall on an Oscillating Airfoil. J. Am. Helicopter Soc., vol. 19, no. 1, January 1974, pp. 26-32.

4. Parker, A. G.; and Bicknell, J.: Some Measurements on Dynamic Stall. J. Aircraft, vol. 11, no. 7, July 1974, pp. 371-374.

5. McCroskey, W. J.; Carr, L. W.; and McAlister, K. W.: Dynamic Stall Experiments on Oscillating Airfoils. AIAA Paper no. 75-125, January 1975.

6. Ham, N. D.: Aerodynamic Loading on a Two-Dimensional Airfoil During Dynamic Stall. AIAA J., vol. 6, no. 10, October 1968, pp. 1927-1934.

7. Ericsson, L.; and Reding, J.: Unsteady Airfoil Stall. NASA CR-66787, July 1969.

8. Crimi, P.; and Reeves, B. L.: A Method for Analyzing Dynamic Stall of Helicopter Rotor Blades. NASA CR-2009, May 1972.

9. Crimi, P.: Investigation of Nonlinear Inviscid and Viscous Flow Effects in the Analysis of Dynamic Stall. NASA CR-2335, February 1974.

10. McCroskey, W. J.; and Fisher, R. K.: Detailed Aerodynamic Measurements on a Model Rotor in the Blade Stall Regime. J. Am. Helicopter Soc., vol. 17, no. 1, January 1972, pp. 20-30.

11. Scheiman, J.: A Tabulation of Helicopter Rotor-Blade Differential Pressures, Stresses, and Motions as Measured in Flight. NASA TM X-952, March 1964.

12. Adams, D. O.: The Evaluation of a Stall-Flutter Spring-Damper Pushrod in the Rotating Control System of a CH-54B Helicopter. USAAMRDL Tech. Rept. no. 73-55, August 1973.

13. Beno, E. A.: Analysis of Helicopter Maneuver-Loads and Rotor-Loads Flight-Test Data. NASA CR-2225, March 1973.

14. Tarzanin, F. J.: Prediction of Control Loads Due to Blade Stall. J. Am. Helicopter Soc., vol. 17, no. 2, April 1972, pp. 33-46.

15. Carta, F.; and Neibanck, C.: Prediction of Rotor Instability at High Forward Speeds--Vol. III, Stall Flutter. USAAVLABS TR 68-18C, February 1969.

16. Crimi, P.: Analysis of Stall Flutter of a Helicopter Rotor Blade. NASA CR-2322, November 1973.

17. Reeves, B. L.; and Lees, L.: Theory of Laminar Near Wake of Blunt Bodies in Hypersonic Flow. AIAA J., vol. 3, no. 11, November 1965, pp. 2061-2074.

18. Lizak, A. A.: Two-Dimensional Wind-Tunnel Tests of an H-34 Main Rotor Airfoil Section. TREC Tech. Rept. 60-53, September 1960.

19. Gessow, A.; and Meyers, G. C.: The Aerodynamics of the Helicopter. Ungar, New York, 1967.

20. Gregory, N.; and Walker, W. S.: Wind-Tunnel Tests on the NACA 63A009 Aerofoil with Distributed Suction Over the Nose. ARC R & M No. 2900, September 1952.